Mechanics of Advanced Materials and Structures

ISSN: 1537-6494 (Print) 1537-6532 (Online) Journal homepage: https://www.tandfonline.com/loi/umcm20

Isogeometric Analysis of Laminated Composite Plates Using the Higher-Order Shear Deformation Theory

Chien H. Thai, H. Nguyen-Xuan, S. P. A. Bordas, N. Nguyen-Thanh & T. Rabczuk

To cite this article: Chien H. Thai, H. Nguyen-Xuan, S. P. A. Bordas, N. Nguyen-Thanh & T. Rabczuk (2015) Isogeometric Analysis of Laminated Composite Plates Using the Higher-Order Shear Deformation Theory, Mechanics of Advanced Materials and Structures, 22:6, 451-469, DOI: 10.1080/15376494.2013.779050

To link to this article: https://doi.org/10.1080/15376494.2013.779050

Accepted author version posted online: 14 Jan 2015.
Published online: 14 Jan 2015.

Mechanics of Advanced Materials and Structures (2015) **22**, 451–469

ISSN: 1537-6494 print / 1537-6532 online
DOI: 10.1080/15376494.2013.779050

Taylor & Francis
Taylor & Francis Group

Isogeometric Analysis of Laminated Composite Plates Using the Higher-Order Shear Deformation Theory

CHIEN H. THAI[1,2], H. NGUYEN-XUAN[3,4], S. P. A. BORDAS[5], N. NGUYEN-THANH[6], and T. RABCZUK[6]

[1]*Division of Computational Mechanics, Ton Duc Thang University, Ho Chi Minh City, Vietnam*
[2]*Faculty of Civil Engineering, Ton Duc Thang University, Ho Chi Minh City, Vietnam*
[3]*Department of Computational Engineering, Vietnamese-German University, Binh Duong New City, Vietnam*
[4]*Department of Architectural Engineering, Sejong University, Seoul, South Korea*
[5]*Institute of Mechanics and Advanced Materials, School of Engineering, College of Physical Sciences, Cardiff University, Wales, UK*
[6]*Institute of Structural Mechanics, Bauhaus-University Weimar, Weimar, Germany*

Received 20 January 2012; accepted 11 December 2012.

Isogeometric analysis (IGA) aims at simplifying the computer aided design (CAD) and computer aided engineering (CAE) pipeline by using the same functions to describe the geometry (CAD) and the unknown fields (Analysis). IGA can be based on a variety of CAD descriptions, the most widely used today being non-uniform rational B-splines (NURBS). In this article, the suitability of NURBS-based isogeometric analysis within a third-order shear deformation theory for the simulation of the static, dynamic, and buckling response of laminated composite plates is investigated. The method employs NURBS basis functions to both represent the geometry (exactly) and the unknown field variables. One of the main advantages of the present method is directly inherited from IGA, that is to easily increase the approximation order. To avoid using a shear correction factor, a third-order shear deformation theory (TSDT) is introduced. It requires C^1-continuity of generalized displacements and the NURBS basis functions are well suited for this requirement. Several numerical examples are used to demonstrate the performance of the present method compared with other published ones.

Keywords: isogeometric analysis, laminated composite plates, third-order shear deformation theory

1. Introduction

Laminated composite plates are widely used in practice, from civil to aerospace engineering. Kinematic representations of such structures are numerous, whether the layers are described implicitly or in an average sense and reliable continuum models exist for the pre-failure regime. Yet, the design and optimization of such structures still requires heavy human intervention, mainly because of the need to discretize potentially complex geometries into finite element representations. Such difficulties are compounded by the iterative nature of the design process. For the analysis of laminated plates, several analytical solutions have been proposed by Pagano [1], Srinivas et al. [2], Srinivas and Rao [3], and Vel and Batra [4] to predict accurately their structural and dynamical behavior. Noor [5, 6] first recommended a three-dimensional (3D) elasticity theory to improve the accuracy of transverse shear stresses. When 3D continuum elements are used to describe the response of these thin structures, the control of the computational cost can become a serious issue.

To reduce this computational cost, many equivalent single layer (ESL) plate theories have been then proposed to transform the 3D problems into a quasi-2D problem. Several plate theories using ESL have been developed to analyze laminated composite plates. The classical laminate plate theory (CLPT) [7–9] can only give good results to thin plates because it ignores the transverse shear deformation. The first-order shear deformation theory (FSDT) [10, 11] can be applied for both moderately thick and thin plates. This theory assumes that transverse shear stresses are constant through the thickness and a shear correction factor (SCF) is needed to take into account the non-linear distribution of shear stresses. The SCF depends on material constants, the laminate scheme, the geometry, and boundary conditions, which makes this factor difficult to determine.

To bypass the limitations of the FSDT, higher-order shear deformation theories (HSDT) have been developed by Librescu [12], Levinson [13], Bhimaraddi and Stevens [14], Reddy [15], Ren [16], Kant and Pandya [17], and Mohan et al. [18]. To avoid the need for a shear correction factor,

Address correspondence to Hung Nguyen-Xuan, Department of Computational Engineering, Vietnamese-German University, Binh Duong New City, Vietnam. E-mail: hung.nx@vgu.edu.vn
Color versions of one or more of the figures in the article can be found online at www.tandfonline.com/umcm.

HSDT uses higher-order terms in Taylor's series expansion of the displacement fields in the thickness direction. It yields more accurate inter-laminar stress distributions and satisfies the conditions of zero shear stress at the top and bottom surfaces of the plate. This model requires C^1-continuity of the w-displacement as the strain terms contain second-order derivatives of the w-displacement.

In addition, various higher order shear deformation theories were proposed to analyze laminated composite plates, such as the global-local method [19, 20], the sinusoidal shear deformation plate theory by Touratier [21], the exponential shear deformation plate theory by Karama et al. [22], the sin-hyperbolic deformation theory by Soldatos [23], the exponential shear deformation plate theory by Aydogdu [24], the hyperbolic shear deformation theory by Meiche et al. [25], and the variable refined theory [26–28], etc. In this study, we adopt the ESL model through the third-order shear deformation theory proposed by Reddy [15].

Due to the limitation of analytical approaches, various numerical methods have been developed, such as finite elements (FEM) [29, 30], boundary elements (BEM) [31, 32], smoothed finite elements (SFEM) [33–38], meshfree methods [39–44]. Substantial efforts have been made by Hughes group, aiming at integrating computer aided design (CAD) and computer aided engineering (CAE) within an isogeometric analysis framework [45]. The basic idea is to use CAD basis functions for the context of numerical analysis. While the finite element method is most popular in CAE, the most common CAD basis functions are Non uniform rational B-splines (NURBS). Therefore, most studies in isogeometric analysis focus on NURBS-based finite element formulations [46–48]. The major advantage of CAD basis functions (e.g., NURBS) over finite elements is their intrinsic ability to describe a wide class of geometric objects, e.g. conic geometries. Hughes et al. [45, 49] showed that NURBS possess important properties required in numerical analysis, such as non-negativity, partition of unity, linear independence, and local support. Besides their potential to unify CAD and CAE, NURBS-based finite element formulations have other advantages over Lagrange-based polynomial finite elements (FEs). Many examples (see, e.g., the results in [50–54]) have shown that NURBS-based isogeometric FEs give more accurate results than their "standard" FEcounterparts with added flexibility. The higher continuity of the isogeometric formulation can also be exploited in a different context, e.g., for thin plates and thick shells [55–57] or for gradient-based constitutive models [58]. We note that any order of continuity can be created easily with NURBS basis functions through a simple procedure, i.e., knot insertion. Some improved approaches for local adaptive refinement were recently proposed in [59–63]. Additionally, an isogeometric boundary element method [64], which has been recently developed, appears more promising for analyzing mechanics problems.

In this article, a novel numerical approach using a NURBS-based isogeometric approach associated with third-order shear deformation theory (TSDT) is formulated for static, free vibration, and buckling analysis of laminated composite plate structures. A plate model relies on third-order shear deformation theory in which shear correction factors are no longer involved. The NURBS basis functions are used in both geometry representation and analysis. A formulation of generalized displacements using the NURBS basis functions can yield higher-order continuity and, hence, the requirement of C^1-continuity of the TSDT is easily achieved. Several numerical results are illustrated to show the effectiveness of the present method.

The article is arranged as follows: a brief review of the B-spline and NURBS surface is described in Section 2. Section 3 presents a formulation of an isogeometric approximation for laminated composite plates. Several numerical examples are provided in Section 4. Finally, we close our article with some concluding remarks.

2. NURBS-Based Isogeometric Analysis Fundamentals

2.1 *Knot Vectors and Basis Functions*

Let $\Xi = [\xi_1, \xi_2, \ldots, \xi_{n+p+1}]$ be a nondecreasing sequence of parameter values, $\xi_i \leq \xi_{i+1}$, $i = 1, \ldots, n + p$. The ξ_i are called knots, and Ξ is the set of coordinates in the parametric space. If all knots are equally spaced, the knot vector is called uniform. If the first and the last knots are repeated $p + 1$ times, the knot vector is described as open. A B-spline basis function is C^∞ continuous inside a knot span and C^{p-1} continuous at a single knot. A knot value can appear more than once and is then called a multiple knot. At a knot of multiplicity k the continuity is C^{p-k}.

Given a knot vector, the B-spline basis functions $N_{i,p}(\xi)$ of order $p = 0$ are defined recursively on the corresponding knot vector as follows:

$$N_{i,0}(\xi) = \begin{cases} 1 \text{ if} \xi_i \ \leq \xi \ < \xi_{i+1} \\ 0 \quad \text{otherwise.} \end{cases} \tag{1}$$

The basis function is defined by the following recursion formula ($p \geqslant 1$)

$$N_{i,p}(\xi) = \frac{\xi - \xi_i}{\xi_{i+p} - \xi_i} N_{i,p-1}(\xi) + \frac{\xi_{i+p+1} - \xi}{\xi_{i+p+1} - \xi_{i+1}} N_{i+1,p-1}(\xi). \tag{2}$$

For $p = 0$ and 1 the basis functions of isogeometric analysis are identical to those of standard piecewise constant and linear finite elements, respectively. For $p \geq 2$ they are different [45]. In this study, we exploit basis functions with $p \geq 2$.

2.2. *B-Spline Curves and Surface*

The B-spline curve is defined as:

$$\mathbf{C}(\xi) = \sum_{i=1}^{n} N_{i,p}(\xi) \mathbf{P}_i, \tag{3}$$

where $\mathbf{P}_i$ are the control points and $N_{i,p}(\xi)$ is the pth-degree B-spline basis function defined on the open knot vector.

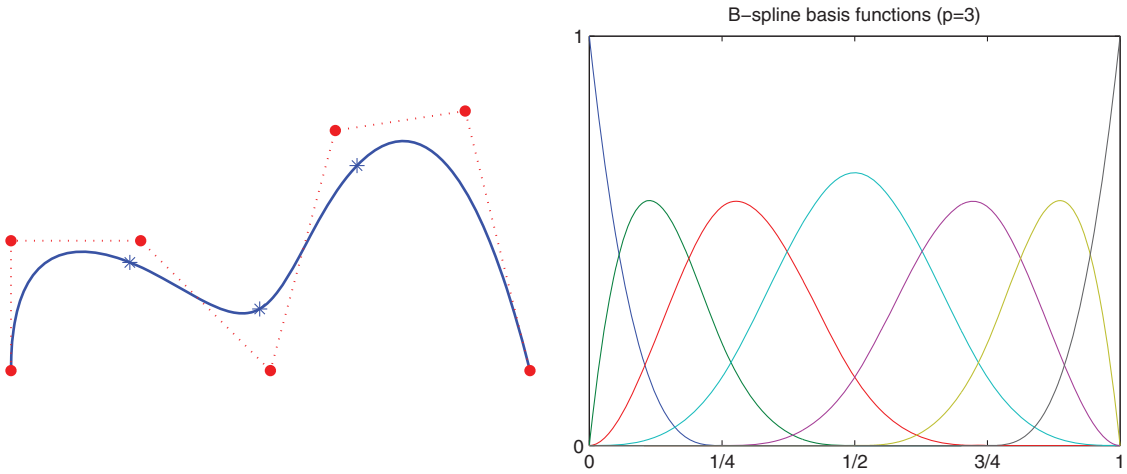

Fig. 1. Cubic B-spline curves and basis functions.

Figure. 1 illustrates a set of cubic B-splines curves and cubic B-spline basis functions for open uniform knot vectors $\Xi = \{0, 0, 0, 0, \frac{1}{4}, \frac{1}{2}, \frac{3}{4}, 1, 1, 1, 1\}$.

The B-spline surfaces are defined by the tensor product of basis functions in two parametric dimensions ξ and η with two knot vectors $\Xi = \{\xi_1, \xi_2 ..., \xi_{n+p+1}\}$ and $\mathrm{H} = \{\eta_1, \eta_2 ..., \eta_{m+q+1}\}$ are expressed as follows:

$$\mathbf{S}(\xi, \eta) = \sum_{i=1}^{n} \sum_{j=1}^{m} N_{i,p}(\xi)\, M_{j,q}(\eta)\, \mathbf{P}_{i,j}, \tag{4}$$

where $\mathbf{P}_{i,j}$ are the bidirectional control net, $N_{i,p}(\xi)$ and $M_{j,q}(\eta)$ are the B-spline basis functions defined on the knot vectors over an $n \times m$ net of control points $\mathbf{P}_{i,j}$.

Similarly to notations used in finite elements, we identify the logical coordinates (i, j) of the B-spline surface with the traditional notation of a node A [55]. Equation (4) can be rewritten in the following form:

$$\mathbf{S}(\xi, \eta) = \sum_{A}^{n \times m} N_A(\xi, \eta)\, \mathbf{P}_A, \tag{5}$$

where $N_A(\xi, \eta) = N_{i,p}(\xi)\, M_{j,q}(\eta)$ is the shape function associated with node A.

Similar to B-splines, a NURBS surface is defined as:

$$\mathbf{S}(\xi, \eta) = \sum_{A}^{n \times m} R_A(\xi, \eta)\, \mathbf{P}_A; \qquad R_A = \frac{N_A \zeta_A}{\sum_{A}^{n \times m} N_A \zeta_A}, \tag{6}$$

where ζ_A are the weight functions. An example of a cubic NURBS surface is provided in Figure. 2.

3. An Isogeometric Formulation for Laminated Composite Plates Using Third-Order Shear-Deformation Plate Theory

3.1. *The Displacements, Strains and Stresses in Plates*

Let Ω be the domain in $\mathbb{R}^2$ occupied by the mid-plane of the plate and u_0, v_0, w_0 and $\boldsymbol{\beta} = (\beta_x, \beta_y)^T$ denote the displacement components in the x, y, z directions and the rotations in the $y - z$ and $x - z$ planes, respectively see Figure 3. The third-order displacement fields are given by Reddy [30]:

$$\begin{aligned} u(x, y, z) &= u_0 + z\beta_x + cz^3 \left(\beta_x + \tfrac{\partial w}{\partial x}\right) \\ v(x, y, z) &= v_0 + z\beta_y + cz^3 \left(\beta_y + \tfrac{\partial w}{\partial y}\right), \\ w(x, y) &= w_0, \end{aligned} \tag{7}$$

where $c = -4/3h^2$.

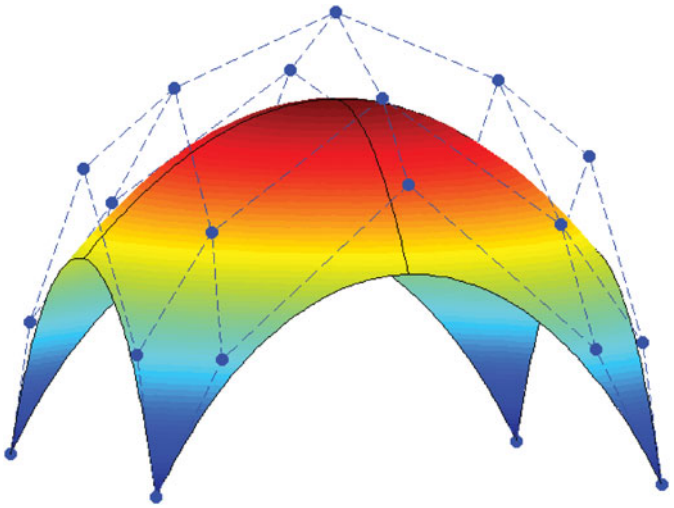

Fig. 2. NURBS surface and control mesh.

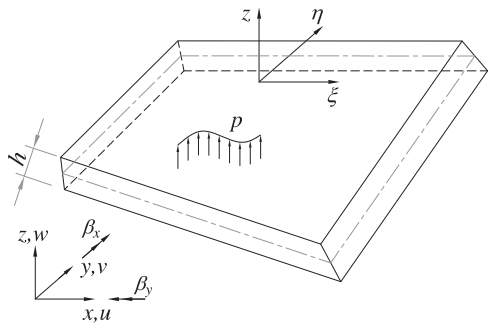

Fig. 3. Geometry of a plate.

The in-plane strain vector $\boldsymbol{\varepsilon}_p = [\varepsilon_{xx}\ \varepsilon_{yy}\ \gamma_{xy}]^T$ can be rewritten as:

$$\boldsymbol{\varepsilon}_p = \boldsymbol{\varepsilon}_0 + z\boldsymbol{\kappa}_1 + z^3\boldsymbol{\kappa}_2, \tag{8}$$

where

$$\boldsymbol{\varepsilon}_0 = \begin{bmatrix} \dfrac{\partial u_0}{\partial x} \\ \dfrac{\partial v_0}{\partial y} \\ \dfrac{\partial u_0}{\partial y} + \dfrac{\partial v_0}{\partial x} \end{bmatrix}, \quad \boldsymbol{\kappa}_1 = \begin{bmatrix} \dfrac{\partial \beta_x}{\partial x} \\ \dfrac{\partial \beta_y}{\partial y} \\ \dfrac{\partial \beta_x}{\partial y} + \dfrac{\partial \beta_y}{\partial x} \end{bmatrix},$$

$$\boldsymbol{\kappa}_2 = c \begin{bmatrix} \dfrac{\partial \beta_x}{\partial x} + \dfrac{\partial^2 w}{\partial x^2} \\ \dfrac{\partial \beta_y}{\partial y} + \dfrac{\partial^2 w}{\partial y^2} \\ \dfrac{\partial \beta_x}{\partial y} + \dfrac{\partial \beta_y}{\partial x} + 2\dfrac{\partial^2 w}{\partial x \partial y} \end{bmatrix},$$

and the transverse shear strain vector $\boldsymbol{\gamma} = [\gamma_{xz}\ \ \gamma_{yz}]^T$ has the form:

$$[\gamma_{xz}\ \ \gamma_{yz}]^T = \boldsymbol{\varepsilon}_s + z^2\boldsymbol{\kappa}_s, \tag{9}$$

where

$$\boldsymbol{\varepsilon}_s = \begin{bmatrix} \beta_x + \dfrac{\partial w}{\partial x} \\ \beta_y + \dfrac{\partial w}{\partial y} \end{bmatrix}, \qquad \boldsymbol{\kappa}_s = 3c \begin{bmatrix} \beta_x + \dfrac{\partial w}{\partial x} \\ \beta_y + \dfrac{\partial w}{\partial y} \end{bmatrix}.$$

The constitutive equation of an orthotropic layer in the local coordinate system is derived from Hooke's law for plane stress by:

$$\begin{Bmatrix} \sigma_{xx} \\ \sigma_{yy} \\ \tau_{xy} \\ \tau_{xz} \\ \tau_{yz} \end{Bmatrix}^{(k)} = \begin{bmatrix} Q_{11} & Q_{12} & Q_{16} & 0 & 0 \\ Q_{21} & Q_{22} & Q_{26} & 0 & 0 \\ Q_{61} & Q_{62} & Q_{66} & 0 & 0 \\ 0 & 0 & 0 & Q_{55} & Q_{54} \\ 0 & 0 & 0 & Q_{45} & Q_{44} \end{bmatrix}^{(k)} \begin{Bmatrix} \varepsilon_{xx} \\ \varepsilon_{yy} \\ \gamma_{xy} \\ \gamma_{xz} \\ \gamma_{yz} \end{Bmatrix}^{(k)}, \tag{10}$$

where material constants are given as:

$$Q_{11} = \frac{E_1}{1-\nu_{12}\nu_{21}},\ Q_{12} = \frac{\nu_{12}E_2}{1-\nu_{12}\nu_{21}},\ Q_{22} = \frac{E_2}{1-\nu_{12}\nu_{21}},$$
$$Q_{66} = G_{12},\ \ Q_{55} = G_{13},\ \ Q_{44} = G_{23}, \tag{11}$$

where E_1, E_2 are the Young modulus in the 1 and 2 directions, respectively, and G_{12}, G_{23}, G_{13} are the shear modulus in the 1-2, 2-3, 3-1 plane, respectively, and ν_{12} and ν_{21} are Poisson's ratios.

The laminate is usually made of several orthotropic layers. Each layer must be transformed to the laminate coordinate system (x, y, z). The stress–strain relationship is given as:

$$\begin{Bmatrix} \sigma_{xx} \\ \sigma_{yy} \\ \tau_{xy} \\ \tau_{xz} \\ \tau_{yz} \end{Bmatrix}^{(k)} = \begin{bmatrix} \bar{Q}_{11} & \bar{Q}_{12} & \bar{Q}_{16} & 0 & 0 \\ \bar{Q}_{21} & \bar{Q}_{22} & \bar{Q}_{26} & 0 & 0 \\ \bar{Q}_{61} & \bar{Q}_{62} & \bar{Q}_{66} & 0 & 0 \\ 0 & 0 & 0 & \bar{Q}_{55} & \bar{Q}_{54} \\ 0 & 0 & 0 & \bar{Q}_{45} & \bar{Q}_{44} \end{bmatrix}^{(k)} \begin{Bmatrix} \varepsilon_{xx} \\ \varepsilon_{yy} \\ \gamma_{xy} \\ \gamma_{xz} \\ \gamma_{yz} \end{Bmatrix}^{(k)}, \tag{12}$$

where $\bar{Q}_{ij}$ is transformed material constant (see [29] for more detail).

3.2. *Weak Form*

A weak form of the static model for composite plates using TSDT can be briefly expressed as:

$$\int_\Omega \delta\boldsymbol{\varepsilon}_p^T \bar{\mathbf{D}} \boldsymbol{\varepsilon}_p \mathrm{d}\Omega + \int_\Omega \delta\boldsymbol{\gamma}^T \bar{\mathbf{D}}_s \boldsymbol{\gamma} \mathrm{d}\Omega = \int_\Omega \delta w_0 p \mathrm{d}\Omega, \tag{13}$$

where p, $\boldsymbol{\varepsilon}_p = \left[\varepsilon_p\ \boldsymbol{\kappa}_1\ \boldsymbol{\kappa}_2\right]^T$ and $\boldsymbol{\gamma} = \left[\boldsymbol{\varepsilon}_s\ \boldsymbol{\kappa}_s\right]^T$ are the transverse loading per unit area, in-plane strains, and transverse shear strains vector, respectively, and

$$\bar{\mathbf{D}} = \begin{bmatrix} \mathbf{A} & \mathbf{B} & \mathbf{E} \\ \mathbf{B} & \mathbf{D} & \mathbf{F} \\ \mathbf{E} & \mathbf{F} & \mathbf{H} \end{bmatrix}, \bar{\mathbf{D}}_s = \begin{bmatrix} \mathbf{A}^s & \mathbf{B}^s \\ \mathbf{B}^s & \mathbf{D}^s \end{bmatrix},$$

$$\left(\mathbf{A}_{ij}, \mathbf{B}_{ij}, \mathbf{D}_{ij}, \mathbf{E}_{ij}, \mathbf{F}_{ij}, \mathbf{H}_{ij}\right) = \int_{-h/2}^{h/2} \left(1, z, z^2, z^3, z^4, z^6\right) Q_{ij} \mathrm{d}z \qquad (i, j = 1, 2, 6),$$

$$\left(\mathbf{A}_{ij}^s, \mathbf{B}_{ij}^s, \mathbf{D}_{ij}^s\right) = \int_{-h/2}^{h/2} \left(1, z^2, z^4\right) Q_{ij} \mathrm{d}z \qquad (i, j = 4, 5).$$

For the free vibration analysis of composite plates using the TSDT, a weak form may be derived from the dynamic form of the principle of virtual work:

$$\int_\Omega \delta\boldsymbol{\varepsilon}_p^T \bar{\mathbf{D}} \boldsymbol{\varepsilon}_p \mathrm{d}\Omega + \int_\Omega \delta\boldsymbol{\gamma}^T \bar{\mathbf{D}}_s \boldsymbol{\gamma} \mathrm{d}\Omega = \int_\Omega \delta\mathbf{u}^T \mathbf{m}\ddot{\mathbf{u}} \mathrm{d}\Omega, \tag{14}$$

where

$$\mathbf{m} = \begin{bmatrix} I_1 & I_2 & cI_4 \\ I_2 & I_3 & cI_5 \\ cI_4 & cI_5 & c^2 I_7 \end{bmatrix}, \quad (I_1, I_2, I_3, I_4, I_5, I_7)$$
$$= \int_{-h/2}^{h/2} \rho \left(1, z, z^2, z^3, z^4, z^6\right) \mathrm{d}z,$$

in which $\mathbf{u} = \left[\mathbf{u}_1\ \mathbf{u}_2\ \mathbf{u}_3\right]^T$ and

$$\mathbf{u}_1 = \begin{bmatrix} u_0 \\ v_0 \\ w_0 \end{bmatrix}, \quad \mathbf{u}_2 = \begin{bmatrix} \beta_x \\ \beta_y \\ 0 \end{bmatrix}; \quad \mathbf{u}_3 = c \begin{bmatrix} \beta_x + \frac{\partial w}{\partial x} \\ \beta_y + \frac{\partial w}{\partial y} \\ 0 \end{bmatrix}.$$

In the case of in-plane buckling analysis and assuming pre-buckling stresses $\hat{\boldsymbol{\sigma}}_0$, nonlinear strains are taken into account in the weak form as:

$$\int_\Omega \delta\boldsymbol{\varepsilon}_p^T \bar{\mathbf{D}} \boldsymbol{\varepsilon}_p d\Omega + \int_\Omega \delta\boldsymbol{\gamma}^T \bar{\mathbf{D}}_s \boldsymbol{\gamma} d\Omega + h \int_\Omega \nabla^T \delta w \hat{\boldsymbol{\sigma}}_0 \nabla w d\Omega = 0, \tag{15}$$

where $\nabla^T = [\partial/\partial x \quad \partial/\partial y]$ and $\hat{\boldsymbol{\sigma}}_0 = \begin{bmatrix} \sigma_x^0 & \tau_{xy}^0 \\ \tau_{xy}^0 & \sigma_y^0 \end{bmatrix}$ are the gradient operator and in-plane pre-buckling stresses, respectively.

Using NURBS basis functions, the field variables are the in-plane extensions, transverse deflection, and the rotations at all control points, which can be expressed as:

$$\mathbf{u}_0 = \begin{Bmatrix} u_0 \\ v_0 \\ w_0 \\ \beta_x \\ \beta_y \end{Bmatrix} = \sum_{A=1}^{n\times m} \begin{bmatrix} R_A & 0 & 0 & 0 & 0 \\ 0 & R_A & 0 & 0 & 0 \\ 0 & 0 & R_A & 0 & 0 \\ 0 & 0 & 0 & R_A & 0 \\ 0 & 0 & 0 & 0 & R_A \end{bmatrix} \begin{Bmatrix} u_A \\ v_A \\ w_A \\ \beta_{xA} \\ \beta_{yA} \end{Bmatrix} = \sum_{A=1}^{n\times m} \mathbf{R}_A \mathbf{q}_A \tag{16}$$

where $n \times m$ is the number basis functions, $\mathbf{R}_A$ and $\mathbf{q}_A = [u_A \quad v_A \quad w_A \quad \beta_{xA} \quad \beta_{yA}]^T$ are rational basis functions and the degrees of freedom of $\mathbf{u}_0$ associated with a control point A, respectively.

The in-plane strains, shear strains, and geometrical strains are written as:

$$[\boldsymbol{\varepsilon}_p\ \boldsymbol{\gamma}]^T = \sum_{A=1}^{n\times m} \left[\mathbf{B}_A^m\ \mathbf{B}_A^{b1}\ \mathbf{B}_A^{b2}\ \mathbf{B}_A^{s0}\ \mathbf{B}_A^{s1}\right] q_A = \sum_{A=1}^{n\times m} \mathbf{B}_A \mathbf{q}_A;$$
$$\boldsymbol{\varepsilon}_g = \sum_{A=1}^{n\times m} \mathbf{B}_A^g \mathbf{q}_A, \tag{17}$$

where

$$\mathbf{B}_A^m = \begin{bmatrix} R_{A,x} & 0 & 0 & 0 & 0 \\ 0 & R_{A,y} & 0 & 0 & 0 \\ R_{A,y} & R_{A,x} & 0 & 0 & 0 \end{bmatrix},$$
$$\mathbf{B}_A^{b1} = \begin{bmatrix} 0 & 0 & 0 & R_{A,x} & 0 \\ 0 & 0 & 0 & 0 & R_{A,y} \\ 0 & 0 & 0 & R_{A,y} & R_{A,x} \end{bmatrix},$$
$$\mathbf{B}_A^{b2} = c \begin{bmatrix} 0 & 0 & R_{A,xx} & R_{A,x} & 0 \\ 0 & 0 & R_{A,yy} & 0 & R_{A,y} \\ 0 & 0 & 2R_{A,xy} & R_{A,y} & R_{A,x} \end{bmatrix}$$

and

$$\mathbf{B}_A^{s0} = \begin{bmatrix} 0 & 0 & R_{A,x} & R_A & 0 \\ 0 & 0 & R_{A,y} & 0 & R_A \end{bmatrix}, \quad \mathbf{B}_A^{s1} = 3c \begin{bmatrix} 0 & 0 & R_{A,x} & R_A & 0 \\ 0 & 0 & R_{A,y} & 0 & R_A \end{bmatrix},$$
$$\mathbf{B}_A^g = \begin{bmatrix} 0 & 0 & R_{A,x} & 0 & 0 \\ 0 & 0 & R_{A,y} & 0 & 0 \end{bmatrix}$$

$$\mathbf{B}_A = \left[\mathbf{B}_A^m\ \mathbf{B}_A^{b1}\ \mathbf{B}_A^{b2}\ \mathbf{B}_A^{s0}\ \mathbf{B}_A^{s1}\right].$$

For static analysis, the formulation of a TSDT plate is obtained as:

$$\mathbf{K}\mathbf{q} = \mathbf{f}, \tag{18}$$

For free vibration analysis, we have,

$$\left(\mathbf{K} - \omega^2 \mathbf{M}\right)\mathbf{q} = 0. \tag{19}$$

And for buckling analysis, we write:

$$\left(\mathbf{K} - \lambda_{cr} \mathbf{K}_g\right)\mathbf{q} = 0, \tag{20}$$

where $\mathbf{K}$ is the global stiffness matrix:

$$\mathbf{K} = \int_\Omega \left\{ \begin{bmatrix} \mathbf{B}^m \\ \mathbf{B}^{b1} \\ \mathbf{B}^{b2} \end{bmatrix}^T \begin{bmatrix} \mathbf{A} & \mathbf{B} & \mathbf{E} \\ \mathbf{B} & \mathbf{D} & \mathbf{F} \\ \mathbf{E} & \mathbf{F} & \mathbf{H} \end{bmatrix} \begin{bmatrix} \mathbf{B}^m \\ \mathbf{B}^{b1} \\ \mathbf{B}^{b2} \end{bmatrix} + \begin{bmatrix} \mathbf{B}^{s0} \\ \mathbf{B}^{s1} \end{bmatrix}^T \begin{bmatrix} \mathbf{A}^s & \mathbf{B}^s \\ \mathbf{B}^s & \mathbf{D}^s \end{bmatrix} \begin{bmatrix} \mathbf{B}^{s0} \\ \mathbf{B}^{s1} \end{bmatrix} \right\} d\Omega, \tag{21}$$

$$\mathbf{f} = \int_\Omega p\mathbf{R} d\Omega + \mathbf{f}^b, \tag{22}$$

in which $\mathbf{f}^b$ is the remaining part of $\mathbf{f}$ subjected to prescribed boundary loads and $\mathbf{M}$ is the global mass matrix:

$$\mathbf{M} = \int_\Omega \left\{ \begin{bmatrix} \mathbf{N}_1 \\ \mathbf{N}_2 \\ \mathbf{N}_3 \end{bmatrix}^T \begin{bmatrix} I_1 & I_2 & cI_4 \\ I_2 & I_3 & cI_5 \\ cI_4 & cI_5 & c^2 I_7 \end{bmatrix} \begin{bmatrix} \mathbf{N}_1 \\ \mathbf{N}_2 \\ \mathbf{N}_3 \end{bmatrix} \right\} d\Omega, \tag{23}$$

where

$$\mathbf{N}_1 = \begin{bmatrix} R_A & 0 & 0 & 0 & 0 \\ 0 & R_A & 0 & 0 & 0 \\ 0 & 0 & R_A & 0 & 0 \end{bmatrix}, \mathbf{N}_2 = \begin{bmatrix} 0 & 0 & 0 & R_A & 0 \\ 0 & 0 & 0 & 0 & R_A \\ 0 & 0 & 0 & 0 & 0 \end{bmatrix}$$
$$\mathbf{N}_3 = \begin{bmatrix} 0 & 0 & R_{A,x} & R_A & 0 \\ 0 & 0 & R_{A,y} & 0 & R_A \\ 0 & 0 & 0 & 0 & 0 \end{bmatrix},$$

and the global geometrical stiffness matrix $\mathbf{K}_g$ is:

$$\mathbf{K}_g = \int_\Omega (\mathbf{B}^g)^T \boldsymbol{\tau} \mathbf{B}^g d\Omega, \ \boldsymbol{\tau} = h\hat{\boldsymbol{\sigma}}_0, \tag{24}$$

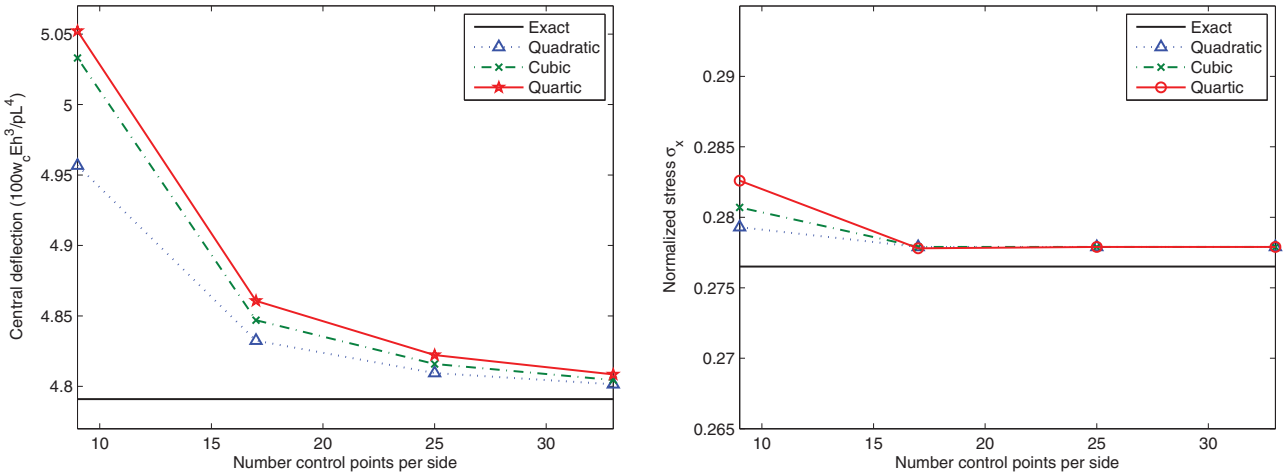

Fig. 4. Simply supported isotropic square plate ($L/h = 10$).

in which ρ, h, ω, and λ_{cr} are the mass density, the thickness, the natural frequency, and the critical buckling load, respectively.

4. Numerical Results

In this section, several numerical examples for both isotropic and composite plates using the TSDT are given. The Quadratic element is defined from the original knot vector $\Xi \times H$. The Cubic and Quartic NURBS elements are obtained by order elevation of the quadratic NURBS basis function based on the coarsest mesh. An h-refinement algorithm is used to generate meshes for all polynomial orders. In all numerical calculations, 3×3, 4×4, and 5×5 integration points are used for the quadratic, cubic, and quartic elements, respectively. The material parameters are assumed as:

- Material I: $E_1 = 25E_2; G_{12} = G_{13} = 0.5E_2; G_{23} = 0.2E_2; \nu_{12} = 0.25$
- Material II: $E_1/E_2 = 10, 20, 30, 40$; $G_{12} = G_{13} = 0.6E_2$; $G_{23} = 0.5E_2$; $\nu_{12} = 0.25$; $\rho = 1$
- Isotropic material: $E_1 = E_2 = 1; G_{12} = G_{13} = G_{23} = E_2/2(1+\nu); \nu = 0.25; \rho = 1$

It is worth mentioning that the NURBS basis functions are noninterpolatory, but the NURBS basis functions using open knot vector have a unity value at first and last points. The NURBS basis functions are, therefore, interpolatory at both end points. If the Dirichlet boundary conditions are homogeneous, these boundary conditions can be directly applied to the control variables. For inhomogeneous Dirichlet boundary conditions, the Lagrange multiplier method [65] can be adopted. In our work, homogeneous condition is used, and thus we can impose directly zero values to the control variables as in the finite element method.

4.1. *Isotropic Plate*

4.1.1. *Static Analysis*

In this problem, we show the performance of the proposed method through static analysis of isotropic plates. Consider a square plate with length L, thickness h, and simply supported boundary conditions, subjected to a uniform load. Length to width ratio is $L/W = 1$ and the length to thickness ratios are given as $L/h = 10, 20, 50, 100$. The material is isotropic. The plate is modeled with 9, 17, 25, and 33 control points per side.

The normalized transverse displacement and bending moment are expressed as:

$$\varpi = (100 \times E_2 \times h^3)\mathrm{w}(\mathrm{L}/2, \mathrm{W}/2, 0)/(\mathrm{qL}^4),$$
$$\bar{\sigma}_{xx} = h^2\sigma_{xx}(L/2, W/2, h/2)/(qL^2).$$

To show the convergence of the present method, we calculate the normalized deflection and stress of the simply supported plates with $L/h = 10$ and a set of of control points as shown in Figure 4. It can be seen that the present solution converges to the exact solution. The quadratic and quartic elements perform best for displacements and stresses, respectively. The normalized central displacement and axial stress of the present method are compared with those of several other approaches, such as the radial basis function-pseudospectral (RBF-PS) using FSDT [66], global radial basis functions (Global) based on HSDT [67], local radial basis functions (Local) based on HSDT [68], FEM based on HSDT [69], and the exact solution [70] as shown in Figure 5. It can be seen that the obtained results are close to the exact solution [70] even for very coarse meshes. Table 1 denotes the present results compared with other published solutions.

4.1.2. *Free Vibration Analysis*

Let us consider a clamped L-shaped isotropic plate with thickness to length ratio $h/a = 0.1$ and Poissons ratio $\nu = 0.3$. The geometry and NURBS meshes are provided in Figure 6. A non-dimensional frequency parameter is defined by $\varpi = (\omega a)(\rho/G)^{1/2}$ with $G = E/2(1+\nu)$. The first four

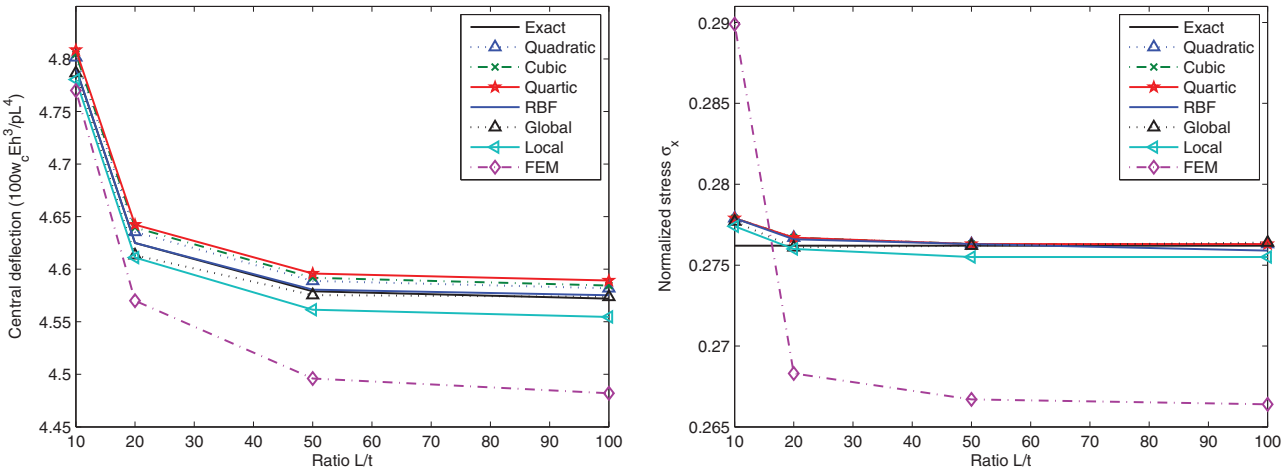

Fig. 5. Simply supported isotropic square plate with various L/h ratios.

Table 1. Square isotropic plate under uniform load

L/h	Method	$\bar{w}$	$\bar{\sigma}_{xx}$
10	Quadratic	4.8015	0.2779
	Cubic	4.8045	0.2779
	Quartic	4.8085	0.2779
	RBF-PS [66]	4.7912	0.2779
	Global [67]	4.7866	0.2777
	Local [68]	4.7804	0.2774
	FEM [69]	4.770	0.2899
	Exact [70]	4.791	0.2762
20	Quadratic	4.6355	0.2767
	Cubic	4.6396	
	Quartic	4.6424	0.2767
	RBF-PS [66]	4.6250	0.2766
	Global [67]	4.6132	0.2761
	Local [68]	4.6110	0.2760
	FEM [69]	4.570	0.2683
	Exact [70]	4.625	0.2762
50	Quadratic	4.5889	0.2763
	Cubic	4.5919	0.2763
	Quartic	4.5959	0.2763
	RBF-PS [66]	4.5805	0.2763
	Global [67]	4.5753	0.2762
	Local [68]	4.5615	0.2755
	FEM [69]	4.496	0.2667
	Exact [70]	4.579	0.2762
100	Quadratic	4.5819	0.2763
	Cubic	4.5844	0.2763
	Quartic	4.5892	0.2763
	RBF-PS [66]	4.5752	0.2759
	Global [67]	4.5737	0.2764
	Local [68]	4.5546	0.2755
	FEM [69]	4.482	0.2664
	Exact [70]	4.572	0.2762

frequency parameters of a clamped L-shaped plate is given in Table 2. The present results are compared with the finite element solution using reduced integration reported by Ferreira [71], a global collocation RBF technique based HSDT presented by Ferreira et al. [67], a local radial basis functions finite difference technique based on HSDT reported in Roque et al. [68], and MITC9/MITC16 elements (mixed interpolated tensorial components) implemented by the authors. It can be seen that the present method produces reasonable results compared with other published methods. The first six mode shapes of the L-shaped plate are shown in Figure 7.

Next, we consider isotropic clamped circular plates. Nondimensional frequency parameters are given by $\varpi = \omega R^2 \sqrt{\frac{\rho h}{D}}$ where $D = \frac{Eh^3}{12(1-\nu^2)}$ is the flexural stiffness. The geometry is shown in Figure 8. A rational quadratic basis is used to represent a circle. The coarsest mesh, $\Xi \times H$, is defined by the knot vectors $\Xi = \{0\,0\,0\,1\,1\,1\}$; $H = \{0\,0\,0\,1\,1\,1\}$. The exact geometry is represented with only one element using nine control points as shown in Figure 9a. The geometric data is given in Table 3. The plate is modeled with a mesh 16×16 NURBS mesh as shown in Figure 9 b. Thin and thick plates are considered in this problem for thickness to radius ratios $h/R = 10, 100$. The results obtained from NURBS are compared with a mesh-free method based on the reproducing kernel particle technique reported by Liew et al. [72], a mesh-free method based on RBF presented by Ferreira et al. [73], finite element method by Hinton [74] and exact solutions in [75]. The first eight frequency parameters of the isotropic clamped circular plate are presented in Table 4. The results obtained from the present method are in excellent agreement with other available ones. The first six mode shapes for the thick clamped circular plate are also plotted in Figure 10.

4.1.3. *Buckling Analysis of Isotropic Plate*

Consider the simply supported plate subjected to in-plane shear as shown in Figure 11. The factors $\bar{\lambda} = \lambda_{cr} b^2 / \left(D_m \pi^2\right)$ of shear buckling loads of this plate are calculated using 17×17 control points per side. The shear buckling load factors with thickness-to-width ratio, $t/b = 0.01$ and length-to-width ratios, $a/b = 1.0, 2.0, 3.0, 4.0$ are shown in Table 5. The present results are compared to the exact solutions in [76] and the meshfree solution of [72]. It is observed that the results of the

Table 2. Nondimensional frequency parameter $\varpi = (\omega a)(\rho / G)^{1/2}$ of a clamped isotropic L-shaped plate

Method	Mesh	ϖ_1	ϖ_2	ϖ_3	ϖ_4	ϖ_5	ϖ_6
Quadratic	8×4	2.0086	2.6169	3.4512	5.0510	5.6495	6.6399
	16×8	1.8497	2.3877	2.7922	3.7112	4.1453	5.1157
	24×12	1.8395	2.3735	2.7507	3.6030	4.0009	4.9635
Cubic	8×4	1.8626	2.3941	2.8504	4.0011	4.5051	5.5105
	16×8	1.8377	2.3704	2.7428	3.5858	3.9826	4.9476
	24×12	1.8369	2.3698	2.7409	3.5791	3.9690	4.9268
Quartic	8×4	1.8414	2.3726	2.7548	3.6408	4.1235	5.1215
	16×8	1.8370	2.3698	2.7409	3.5793	3.9696	4.9298
	24×12	1.8367	2.3696	2.7407	3.5784	3.9678	4.9250
FEM [71]		1.8557	2.3952	2.7637	3.6210	-	-
Global [67]		1.8468	2.3266	2.6806	3.4987	-	-
Local [68]		1.8832	2.3450	2.7698	3.5714	-	-
MITC9		1.8074	2.2633	2.6292	3.4493	-	-
MITC16		1.8397	2.3712	2.7419	3.5827	—	—

quadratic, cubic, and quartic elements agree well with the exact solution. The factor of buckling load of the plate is well approximated using the present method. The shear buckling load decreases rapidly as the length-to-width ratios increases. Figure 12 shows the shear buckling modes of simply-supported rectangular plates with thickness-to-width ratios $t/b = 0.01$ and various length-to-width ratios, $a/b = 1.0; 2.0; 3.0; 4.0$, respectively.

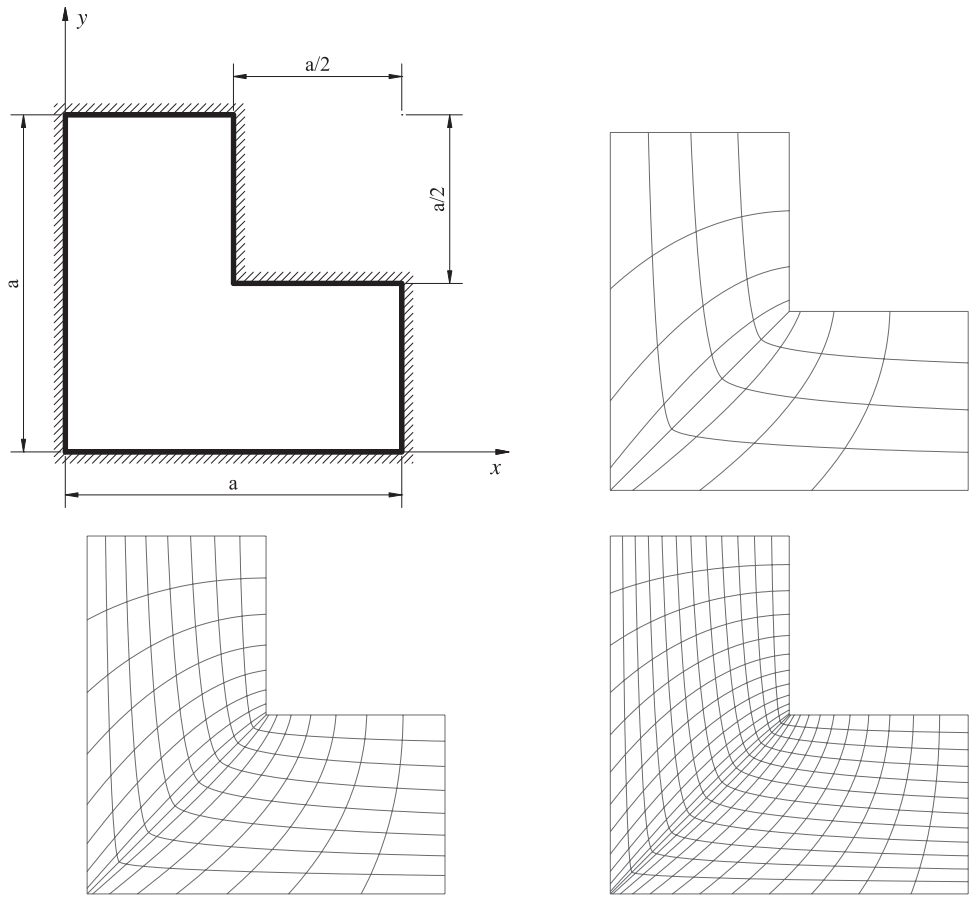

Fig. 6. Geometry and NURBS meshes of L-shape isotropic plate.

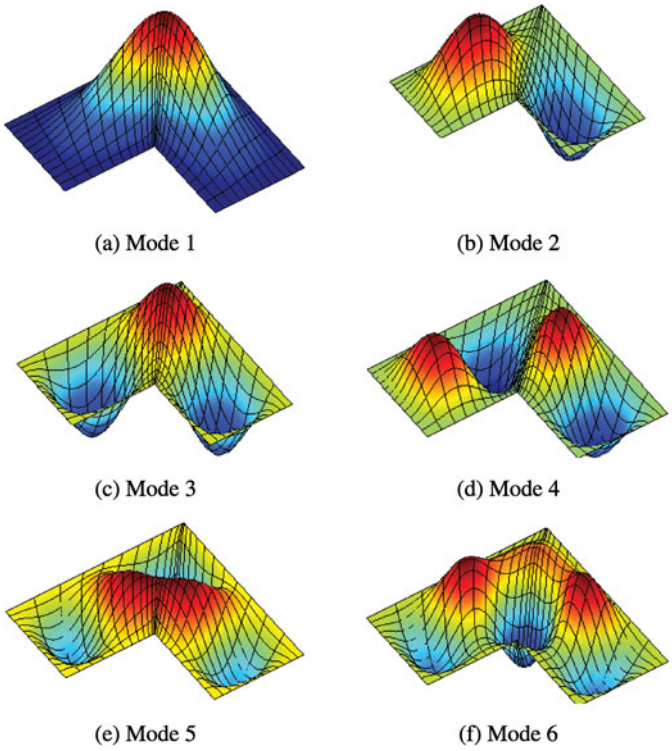

Fig. 7. Mode shapes 1–6 of a clamped *L*-shaped plate using the cubic element.

4.2. *Static Analysis of Laminated Plates*

4.2.1. *Four Layer [0/90/90/0] Square Laminated Plate Under Sinusoidally Distributed Load*

Let us consider a simply supported square laminated plate subjected to a sinusoidal load q as shown in Figure 13. The length to width ratio is $a/b = 1$ and the length to thickness ratio is $a/h = 4, 10, 20, 100$. The plate is modeled by 25×25 control points per side. Material I described previously is used in the numerical calculation.

The normalized displacement and the normal stresses of a square plate are defined as:

$$\varpi = (100E_2h^3)\mathrm{w}(\mathrm{a}/2, \mathrm{a}/2, 0)/(\mathrm{qa}^4),$$

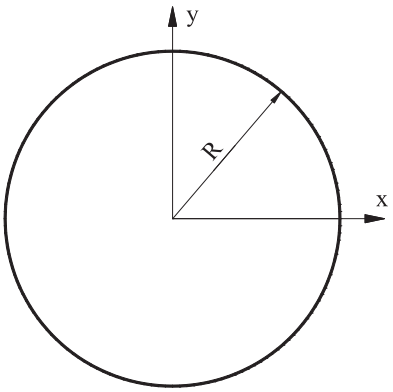

Fig. 8. Geometry of a circular plate.

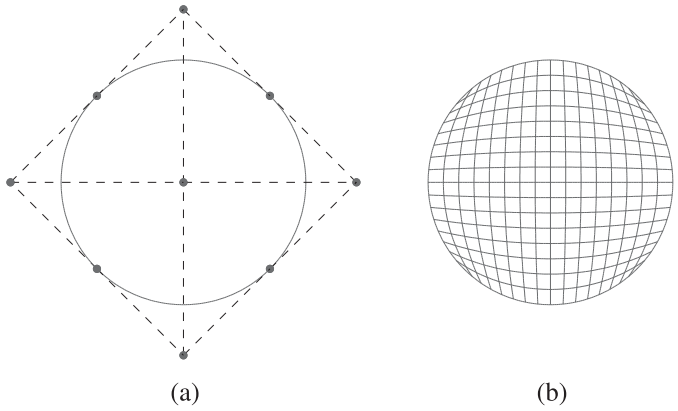

Fig. 9. Circular plate: (a) coarse mesh and control net, and (b) mesh 16×16.

$$\bar{\sigma}_{xx} = \frac{h^2}{qb^2}\sigma_{xx}(a/2, a/2, h/2),$$
$$\bar{\sigma}_{yy} = \frac{h^2}{qb^2}\sigma_{yy}(a/2, a/2, h/4); \bar{\tau}_{xy} = \frac{h^2}{qb^2}\sigma_{xy}(0, 0, h/2),$$

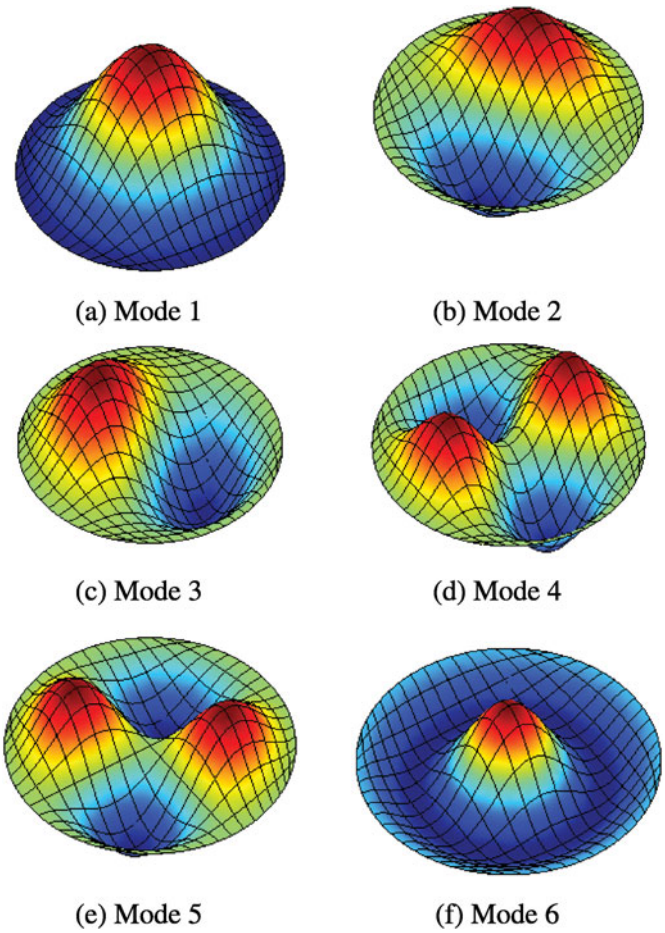

Fig. 10. The first six mode shapes of a isotropic clamped circular plate using cubic element.

Table 3. Control points and weights for a disk of radius 0.5

i	1	2	3	4	5	6	7	8	9
x_i	$-\sqrt{2}/4$	$-\sqrt{2}/2$	$-\sqrt{2}/4$	0	0	0	$\sqrt{2}/4$	$\sqrt{2}/2$	$\sqrt{2}/4$
y_i	$\sqrt{2}/4$	0	$-\sqrt{2}/4$	$\sqrt{2}/2$	0	$-\sqrt{2}/2$	$\sqrt{2}/4$	0	$-\sqrt{2}/4$
w_i	1	$\sqrt{2}/2$	1	$\sqrt{2}/2$	1	$\sqrt{2}/2$	1	$\sqrt{2}/2$	1

$$\bar{\tau}_{xz} = \frac{h}{qb}\sigma_{xy}(0, b/2, 0).$$

The results of the present method are compared with the several other methods including the finite element method (FEM) based on HSDT by Reddy [15], finite strip method (FSM) based on HSDT by Akhras et al. [70], the finite point method (FPM) based on HSDT by Ferreira et al. [77], the node-based smoothed finite element formulation (NS-FEM) based on HSDT by Thai et al. [78], the multiquadrics collocation method (MCM) based on layerwise deformation theory by Ferreira [79], and the elasticity solution given in Pagano [1]. The comparison is provided in Table 6. It is observed that for deflection the result of the NURBS-based method agrees well with the exact solution [1]. For stress analysis, it is close to the solution of the finite strip method using HSDT [70]. Normalized stresses are shown in Figure 14. Figure 15 plots the distribution of stresses through the thickness of the plate with $a/h = 4$, 10, respectively. It is verified that the shear stresses are equal to zeros at boundary edges and distribute discontinuously through laminas. The obtained results are in good agreement with those reported by Reddy [30].

4.2.2. *Three Layer [0/90/0] Square Laminated Plate Under a Uniformly Distributed Load*

Let us consider a simply supported square laminated plate subjected to a uniform load q as shown in Figure. 13. The length to width ratios is a/b =1 and the length to thickness ratios is $a/h = 5$, 10, 20. The plate is modeled 25×25 control points per side. Material I is also used in this problem.

The normalized displacement and the normal stresses of the three layer [0/90/0] square plate are defined as:

$$\begin{aligned}
\varpi &= (100E_2h^3)\mathrm{w}(a/2, a/2, 0)/(qa^4),\\
\bar{\sigma}_{xx} &= \frac{h^2}{qb^2}\sigma_{xx}(a/2, a/2, h/2),\\
\bar{\sigma}_{yy} &= \frac{h^2}{qb^2}\sigma_{yy}(a/2, a/2, h/3);\\
\bar{\tau}_{xy} &= \frac{h^2}{qb^2}\sigma_{xy}(a, b, -h/2),\\
\bar{\tau}_{xz} &= \frac{h}{qb}\sigma_{xy}(0, b/2, h/3);\\
\bar{\tau}_{yz} &= \frac{h}{qb}\sigma_{xy}(a/2, 0, -h/3).
\end{aligned}$$

The results of the present approach are compared with those of the exact approach [30], the element free Galerkin (EFG) using FSDT by Belinha and Dinis [80], 3D-FEM solution by Xiao et al. [81], the meshless local Petrov Galerkin (MLPG) using Multiquadrics(MQ-MLPG) and thin plate splines (TPS-MLPG) based on HSDT by Xiao et al. [81] as shown in Table 7. It is observed that the present solution agrees well with other published results. In particular, it is close to the numerical solution using the meshless local Petrov Galerkin [81].

Table 4. A nondimensional frequency parameter $\varpi = (\omega R^2)(\rho h/D_m)^{1/2}$ of an isotropic clamped circular plate

		Modes							
R/h	Method	1	2	3	4	5	6	7	8
10	*Quadratic*	9.9443	20.1923	32.2417	36.5396	45.8804	54.0131	60.8686	72.4722
	Cubic	9.9439	20.1880	32.2318	36.5118	45.8242	53.9147	60.7231	72.3333
	Quartic	9.9439	20.1880	32.2314	36.5111	45.8223	53.9113	60.7172	72.3280
	RBF [73]	9.9442	20.1884	32.2313	36.5086	45.8353	53.9028	60.7466	72.3012
	Meshfree [72]	9.931	20.194	32.353	36.665	45.827	54.257	60.6595	72.669
	Exact [75]	9.941	20.232	32.406	36.479	46.178	53.89	61.272	72.368
100	Quadratic	10.2242	21.3852	35.1321	40.7500	52.9545	64.8788	74.4369	89.1659
	Cubic	10.2135	21.2554	34.8637	39.7967	51.1153	61.0447	69.9459	84.8685
	Quartic	10.2130	21.2488	34.8470	39.7348	50.9706	60.7532	69.5650	84.4405
	RBF [73]	10.2317	21.2684	34.9802	39.6223	52.1268	60.8731	76.3506	86.8181
	Fem [74]	10.2158	21.2600	34.8800	39.7710	51.0400	60.8200	69.6659	84.58
	Meshfree [72]	10.2661	21.4488	35.2556	40.2905	51.6626	62.1455	70.4145	86.3649

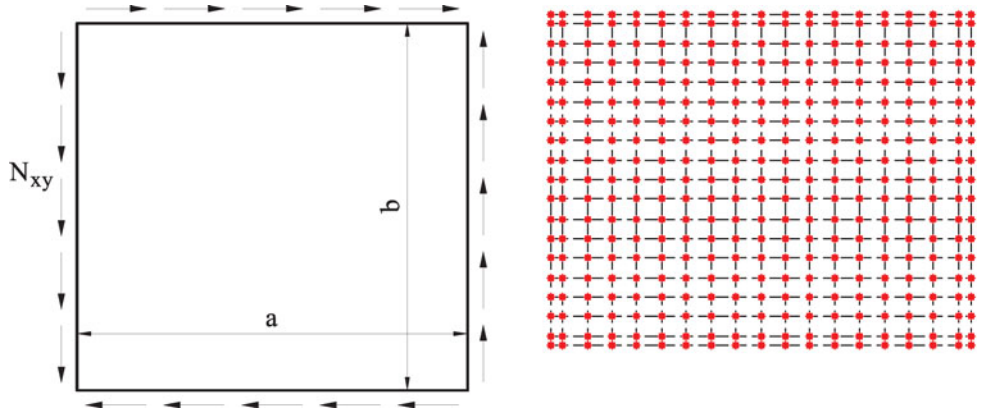

Fig. 11. Geometry and control mesh of a square isotropic plate.

4.3. *Buckling Analysis of Composite Plates*

In this subsection, the buckling load factor is defined as $\bar{\lambda} = \lambda_{cr} a^2 / \left(E_2 h^3\right)$, where a, h, and λ_{cr} are the edge length, thickness of the composite plates, and the critical buckling load, respectively. Material II is used in the examples.

4.3.1. *Square Plate Under uniaxial Compression*

A simply supported four-layer cross-ply $[0^\circ/90^\circ/90^\circ/0^\circ]$ square laminated plate is subjected to uniaxial compression as shown in Figure 16. The span-to-thickness ratio of the plate a/h is taken to be 10. The plate has supported (S), free (F), and clamped (C) edges. The efficiency and accuracy of the present method for various modulus ratios are considered.

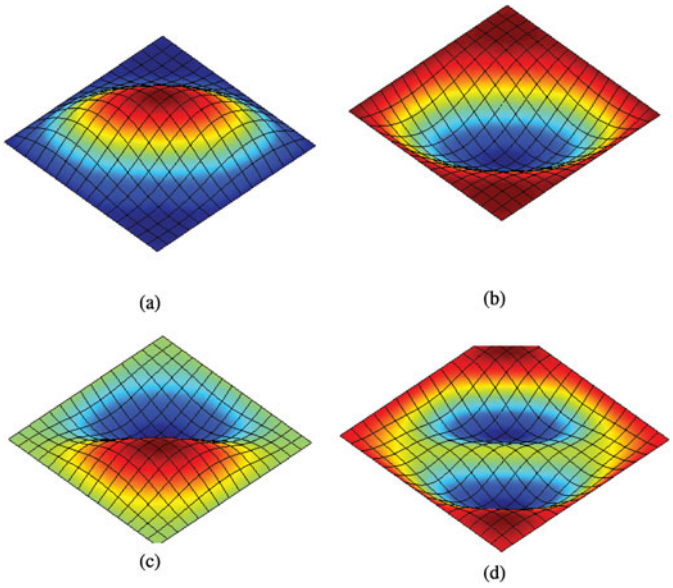

Fig. 12. Shear buckling modes of isotropic simply supported rectangular plates using Quartic elements with various length-to-width ratios: (a) $a/b = 1.0$, (b) $a/b = 2.0$, (c) $a/b = 3.0$, (d) and $a/b = 4.0$.

The convergence of the normalized critical buckling load of a simply supported four-layer cross-ply square laminated with the various modulus ratios is provided in Table 8. The results are compared to the 3D elasticity solution [82], RPIM solution based on HSDT [83], and FEM solution based on HSDT [84, 85]. It is again seen that the present approach shows a good competitor with other methods. It is also observed that the normalized critical buckling loads become larger with increasing of the E_1/E_2 modulus ratios.

Next, the effect of the span-to-thickness ratios (a/h) on the uniaxial compression load is also considered for two- and four-layer simply supported cross-ply square plates. Table 9 illustrates the normalized critical buckling load of two- and four-layer simply supported plates. It is seen that the present result is acceptable to available solutions. In addition, the influence of the mixed boundary conditions of 2 and 10- layer cross-ply square plates is studied. We consider the normalized critical buckling load factors of SSSS, SSFF, SSCC, SSFC, and SSFS plates with length-to-thickness ratios $a/h = 10$ and modulus ratios $E_1/E_2 = 40$. As given in Table 10, the present method is very well compared to several other methods. Figure 17 illustrates buckling shape modes of a 10-layer $[0^\circ/90^\circ]_5$ plate with various boundary conditions.

4.3.2. *Square Plate under Biaxial Compression*

Finally, we consider the three-layer symmetric cross-ply $[0^\circ/90^\circ/0^\circ]$ simply supported plate subjected to the bi-axial buckling load shown in Figure 17. The plate has length a,

Table 5. The shear buckling load factors $\bar{\lambda}$ of simply supported rectangular plates with various length-to-width ratios

a/b	Quadratic	Cubic	Quartic	ES-DSG3 [34]	Meshfree [72]	Exact [76]
1	9.3382	9.3128	9.2903	9.283	9.3962	9.34
2	6.5034	6.5015	6.4945	6.4455	6.3741	6.34
3	5.7455	5.7499	5.7535	5.883	5.7232	5.784
4	5.4647	5.4756	5.4873	5.6732	5.4367	5.59

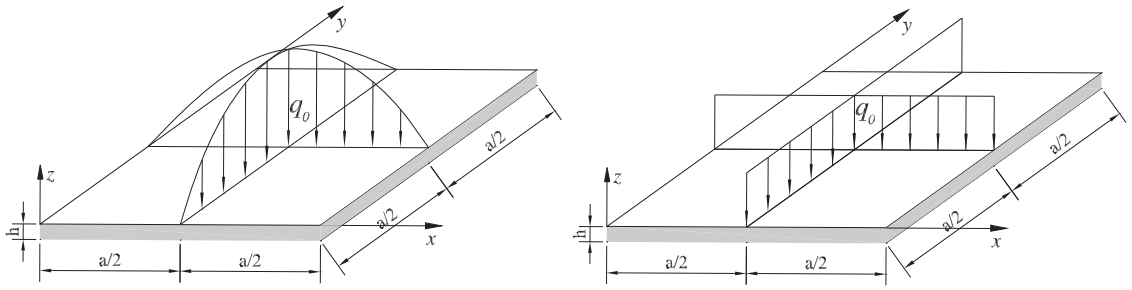

Fig. 13. Geometry of a square laminated plate under sinusoidally and uniformly distributed load.

thickness h, and the span-to-thickness ratio a/h is taken to be 10. The plate is modeled with a control net mesh 17 × 17. The effect of modulus ratio E_1/E_2 and length to thickness ratios a/h on the critical bi-axial buckling load are studied in this section. Table 11 shows the normalized critical buckling loads corresponding to various modulus ratios. When the modulus ratio E_1/E_2 increases, the normalized critical bi-axial buckling loads are also increased. Table 12 illustrates the normalized critical buckling loads with various ratios a/h. It can be seen that the present method works well compared with

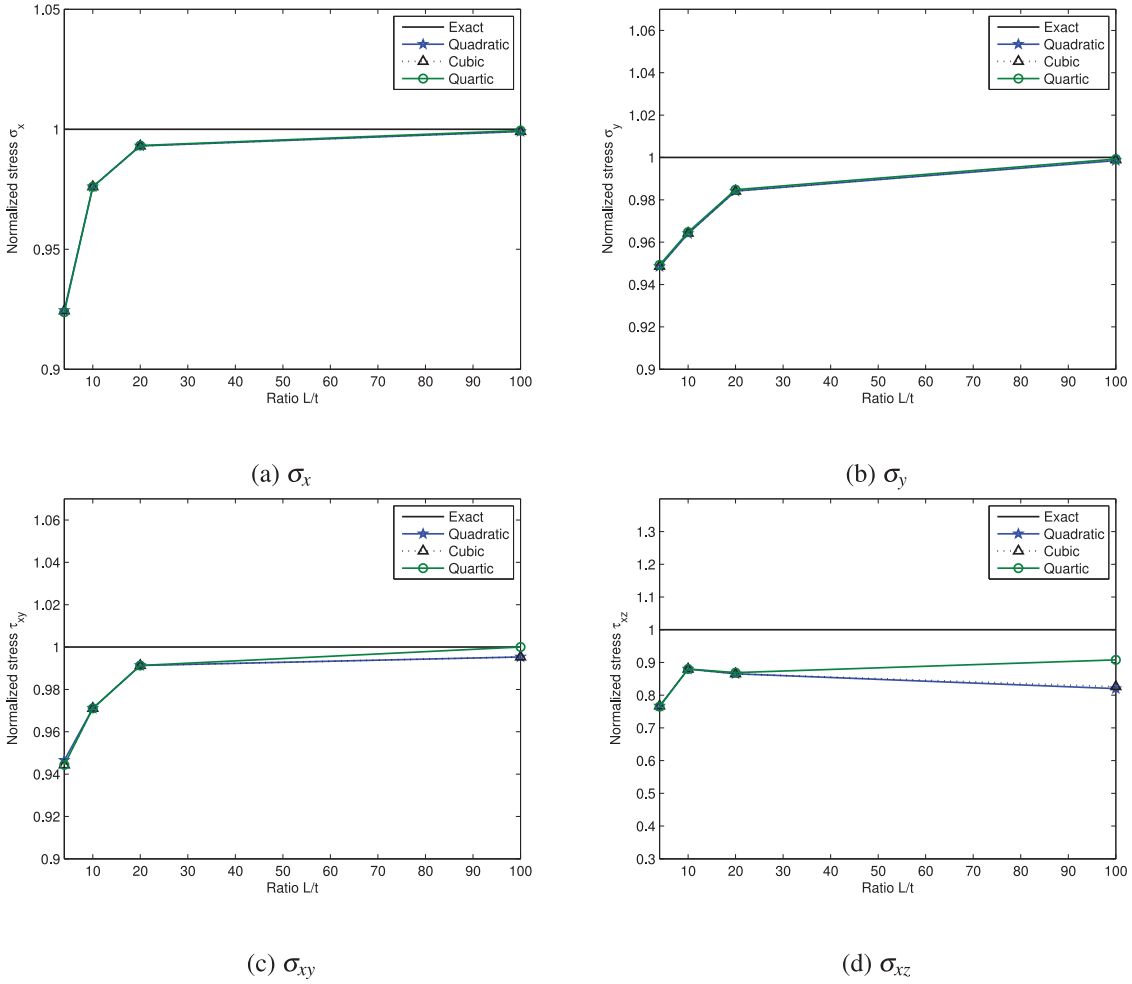

Fig. 14. Normalized stress for four laminated plates.

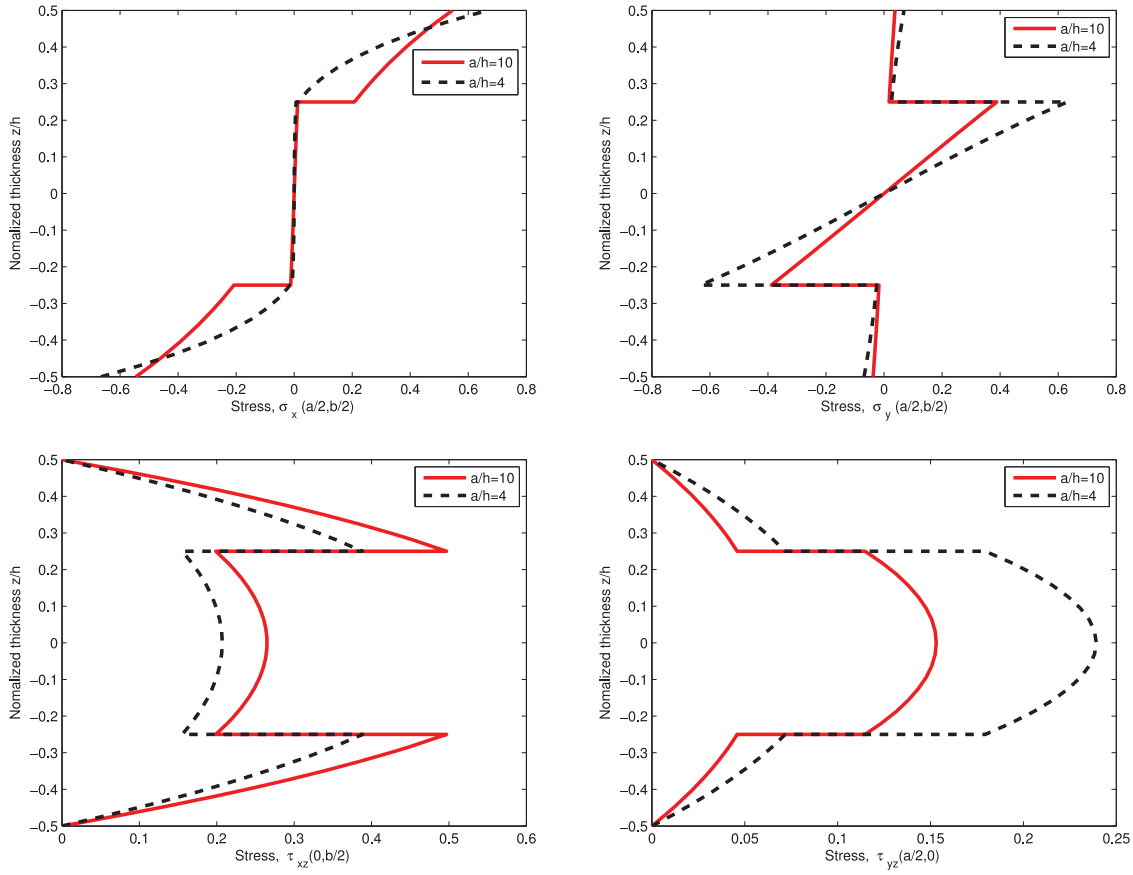

Fig. 15. The distribution of stresses through the thickness of the plate under a sinusoidally distributed load.

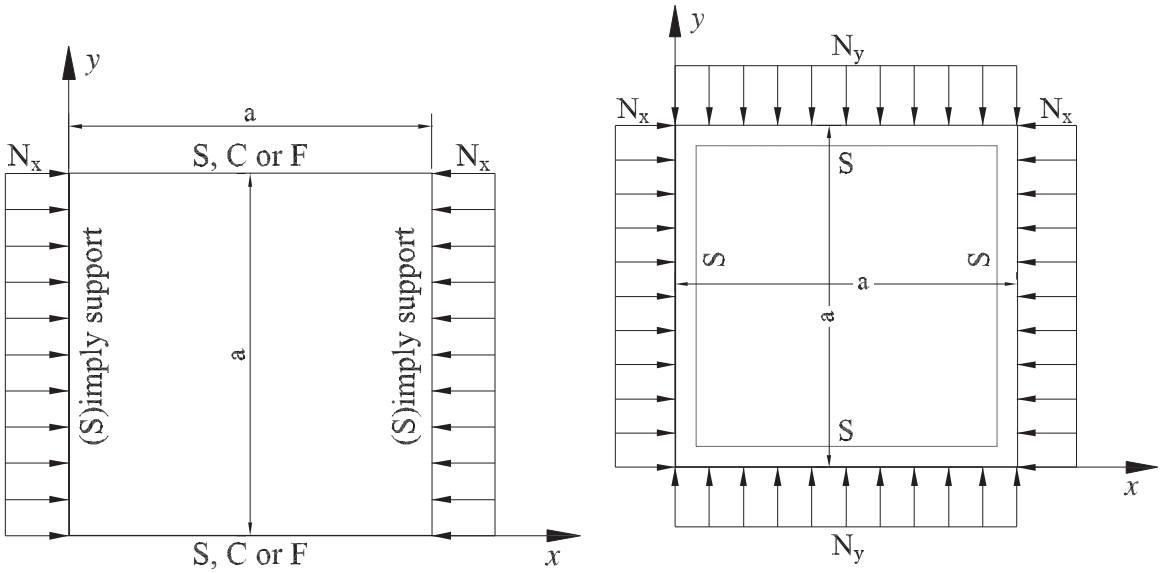

Fig. 16. Geometry of laminated composite plates under axial and biaxial compression.

Table 6. The normalized displacement $\bar{w}$ of a supported simply [0/90/90/0] square laminated plate under a sinusoidally distributed load

a/h	Method	$\bar{w}$	$\bar{\sigma}_{xx}$	$\bar{\sigma}_{yy}$	$\bar{\sigma}_{xz}$	$\bar{\sigma}_{xy}$
4	FEM-HSDT [15]	1.8939	0.6806	0.6463	0.2109	0.0450
	FSM-HSDT [70]	1.8937	0.6651	0.6322	0.2064	0.0440
	FPM-HSDT [77]	1.8864	0.6659	0.6313	0.1352	0.0433
	NS-FEM-HSDT [78]	1.9266	0.7076	0.6303	0.2084	0.0475
	MCM-Layerwise [79]	1.9075	0.6432	0.6228	0.2166	0.0441
	Elasticity [1]	1.954	0.720	0.666	0.270	0.0467
	Quadratic	1.9012	0.6656	0.6317	0.2070	0.0442
	Cubic	1.9001	0.6655	0.6318	0.2070	0.0441
	Quartic	1.9072	0.6651	0.6322	0.2066	0.0441
10	FEM-HSDT [15]	0.7149	0.5589	0.3974	0.2697	0.0273
	FSM-HSDT [70]	0.7147	0.5456	0.3888	0.2640	0.0268
	FPM-HSDT [77]	0.7153	0.5466	0.4383	0.3347	0.0267
	NS-FEM-HSDT [78]	0.7246	0.5609	0.3909	0.2812	0.0288
	MCM-Layerwise [79]	0.7309	0.5496	0.3956	0.2888	0.0273
	Elasticity [1]	0.743	0.559	0.403	0.301	0.0276
	Quadratic	0.7177	0.5456	0.3885	0.2648	0.0268
	Cubic	0.7173	0.5456	0.3886	0.2648	0.0268
	Quartic	0.7199	0.5456	0.3888	0.2649	0.0268
20	FEM-HSDT [15]	0.5061	0.5523	0.311	0.2883	0.0233
	FSM-HSDT [70]	0.506	0.5393	0.3043	0.2825	0.0228
	FPM-HSDT [77]	0.507	0.5405	0.3648	0.3818	0.0228
	NS-FEM-HSDT [78]	0.5089	0.5433	0.3050	0.3051	0.0234
	MCM-Layerwise [79]	0.5121	0.5417	0.3056	0.3248	0.0230
	Elasticity [1]	0.517	0.543	0.309	0.328	0.0230
	Quadratic	0.5082	0.5392	0.3041	0.2838	0.0228
	Cubic	0.5078	0.5392	0.3041	0.2838	0.0228
	Quartic	0.5097	0.5393	0.3043	0.2850	0.0228
100	FEM-HSDT [15]	0.4343	0.5507	0.2769	0.2948	0.0217
	FSM-HSDT [70]	0.4343	0.5387	0.2708	0.2897	0.0213
	FPM-HSDT [77]	0.4365	0.5413	0.3359	0.4106	0.0215
	NS-FEM-HSDT [78]	0.4345	0.5384	0.2706	0.3183	0.0211
	MCM-Layerwise [79]	0.4374	0.542	0.2697	0.3232	0.0216
	Elasticity [1]	0.4347	0.539	0.271	0.339	0.0214
	Quadratic	0.4361	0.5385	0.2706	0.2780	0.0213
	Cubic	0.4358	0.5385	0.2707	0.2801	0.0213
	Quartic	0.4374	0.5387	0.2708	0.3078	0.0214

several other methods for various modulus ratios and length to thickness, respectively.

4.4. *Free Vibration Analysis of Laminated Composite Plates*

Let us consider a four layer [0/90/90/0] simply supported plate, where all layers of the laminated plate are assumed to be of the same thickness and mass density, and made of the same linearly elastic composite material. The material I is used in this section. The thickness to length ratio $h/a = 0.2$ and various modulus ratios $E_1/E_2 = 10, 20, 30, 40$. The first normalized frequencies derived from the present method are listed in Table 13. The results obtained are compared with exact solutions by Reddy and Kdheir [29, 93,] using HSDT, a global method by Ferreira et al. [67] based on HSDT, the local method by Roque et al. [68] based on HSDT, the moving least squares differential quadrature method by Liew et al. [94] using FSDT, radial basis functions by Ferreira [95] based on FSDT, and wavelets by Ferreira et al. [96] using FSDT. It is seen that the present results are acceptable compared to the exact values [29, 93] that are based on high order shear deformation theory.

Next, we consider a three-layer laminate [0/90/0] rectangular supported plate with $E_1/E_2 = 40$. The normalized frequencies are defined as $\varpi = \left(\omega a^2/h\right)\left(\rho/E_2\right)^{1/2}$. The geometry are described: length to width ratios $a/b = 1$ and length to thickness ratios $a/h = 2, 5, 10, 100$. The plate is modeled with 17 control points per side. The present results are compared with solutions reported in Liew [97] based on the FSDT, the finite element method by Reddy [29] using HSDT, as well as radial basis functions by Ferreira et al. [98], and inverse

Table 7. The normalized displacement ϖ of a supported simply [0/90/0] square laminated plate under uniformly distributed load

a/h	Method	$\bar{w}$	$\bar{\sigma}_{xx}$	$\bar{\sigma}_{yy}$	$\bar{\tau}_{xy}$	$\bar{\tau}_{xz}$	$\bar{\tau}_{yz}$
20	3D-FEM [81]	0.7951	0.8247	0.2391	0.0493	0.690	0.3910
	Exact(FSDT) [81]	0.7572	0.7983	0.2227	0.0453	0.7697	0.2902
	EFG(FSDT) [80]	0.7583	0.7905	0.2279	0.0441	0.744	0.2264
	MQ-MLPG(HSDT) [81]	0.7688	0.8125	0.2300	0.0458	1.070	0.3570
	TSP-MLPG(HSDT) [81]	0.7613	0.8050	0.2285	0.0453	1.010	0.3025
	Quadratic	0.7787	0.8159	0.2310	0.0472	1.0222	0.3050
	Cubic	0.7796	0.8159	0.2310	0.0472	1.0236	0.3082
	Quartic	0.7805	0.8161	0.2308	0.0478	1.0411	0.3346
10	3D-FEM [81]	1.1401	0.8280	0.5617	0.0603	0.554	0.498
	Exact(FSDT) [81]	1.0250	0.7577	0.5006	0.047	0.798	0.350
	EFG(FSDT) [80]	1.0248	0.7494	0.4988	0.0458	0.763	0.332
	MQ-MLPG(HSDT) [81]	1.1090	0.8280	0.5480	0.0541	0.949	0.439
	TSP-MLPG(HSDT) [81]	1.0955	0.8240	0.5410	0.0539	0.922	0.430
	Quadratic	1.0937	0.8390	0.5347	0.0584	0.9725	0.3343
	Cubic	1.0950	0.8390	0.5347	0.0585	0.9738	0.3361
	Quartic	1.0963	0.8392	0.5345	0.0596	0.9842	0.3515
5	3D-FEM [81]	2.2383	0.908	0.861	0.1072	0.568	0.4487
	MQ-MLPG(HSDT) [81]	2.1496	0.904	0.820	0.0828	0.424	0.496
	TSP-MLPG(HSDT) [81]	2.1400	0.900	0.816	0.0812	0.796	0.484
	Quadratic	2.1941	0.9361	0.8066	0.0899	0.8440	0.4039
	Cubic	2.1967	0.9361	0.8066	0.0901	0.8448	0.4051
	Quartic	2.1991	0.9361	0.8066	0.0922	0.8495	0.4164

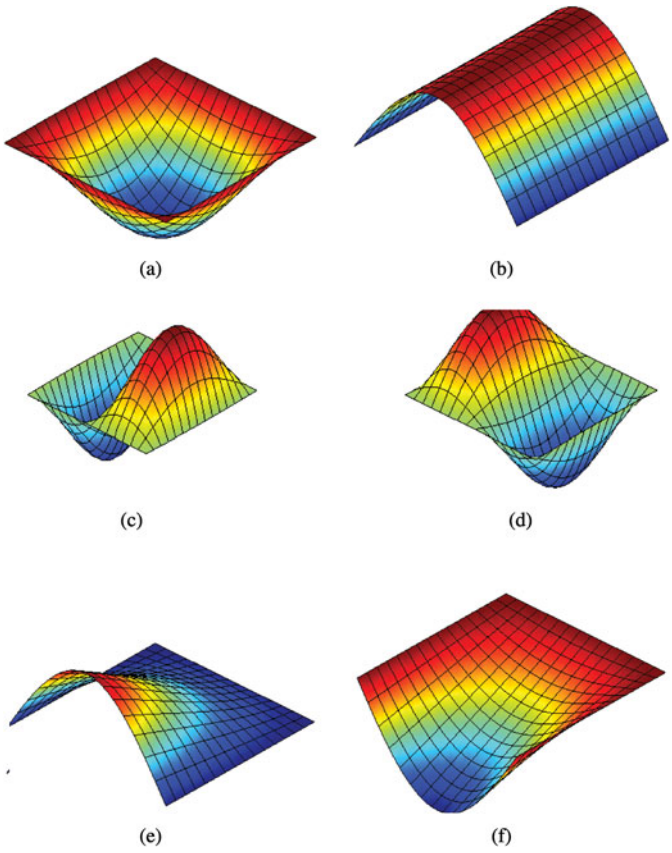

Fig. 17. Fundamental buckling modes of 10-layer $[0°/90°]_5$: (a) SSSS, (b) SSFF, (c) SSCC, (d) SSSC, (e) SSFC, and (f) SSFS.

multiquadric RBF using trigonometric shear deformation theory by Xiang and Wang [99]. The first normalized frequencies of the present method are given in Table 14. It can be seen that the present results are in good agreement with other published results.

Table 8. Normalized critical buckling load of simply supported cross-ply $[0°/90°/90°/0°]$ square plate with various E_1/E_2 ratios

		$E1/E2$				
Method	Mesh	3	10	20	30	40
Quadratic	9×9	5.3903	9.9167	15.2241	19.5382	23.1377
	13×13	5.3871	9.9157	15.2339	19.5633	23.1798
	17×17	5.3876	9.9195	15.2459	19.5852	23.2126
Cubic	9×9	5.3851	9.9058	15.2080	19.5192	23.1174
	13×13	5.3853	9.9116	15.2277	19.5558	23.1716
	17×17	5.3867	9.9174	15.2427	19.5814	23.2082
Quartic	9×9	5.3833	9.9036	15.2061	19.5182	23.1173
	13×13	5.3850	9.9113	15.2276	19.5560	23.1721
	17×17	5.3866	9.9174	15.2427	19.5814	23.2084
Liu [83]		5.412	10.013	15.309	19.778	23.412
Phan [84]		5.114	9.774	15.298	19.957	23.340
Khdeir [85]		5.442	10.026	15.418	19.813	23.489
Noor [82]		5.294	9.762	15.019	19.304	22.881

Table 9. Normalized critical buckling load of simply supported cross-ply square plate with various ratios a/h

Number layer	Method	a/h 10	20	50	100
[0°/90°]	Quadratic	11.5360	12.5794	12.9043	12.9584
	Cubic	11.5315	12.5741	12.8977	12.9472
	Quartic	11.5312	12.5734	12.8959	12.9434
	MISQ20 [86]	11.169	12.520	12.967	13.033
	FSDT [87]	11.349	12.510	12.879	12.934
	FSDT [88]	11.353	12.515	12.884	12.939
	HSDT [88]	11.563	12.577	12.895	12.942
	Quadratic	23.2126	31.6407	35.3607	35.9771
[0°/90°/	Cubic	23.2082	31.6325	35.3497	35.9612
90°/0°]	Quartic	23.2084	31.6318	35.3477	35.9563
	MISQ20 [86]	23.236	31.747	35.561	36.190
	FSDT [87]	23.409	31.625	35.254	35.851
	FSDT [88]	23.471	31.707	35.356	35.955
	HSDT [88]	23.349	31.637	35.419	35.971

Table 12. Biaxial critical buckling load of simply supported cross-ply [0°/90°/0°] square plate with various ratios a/h

Method	a/h 2	5	10	15	20
Quadratic	1.4384	5.4473	10.1096	12.2639	13.3120
Cubic	1.4399	5.4465	10.1046	12.2570	13.3037
Quartic	1.4413	5.4469	10.1040	12.2556	13.3016
TSDT [83]	1.457	5.519	10.251	12.239	13.164
FSDT [83]	1.419	5.484	10.189	12.213	13.132
TSDT [85]	1.465	5.526	10.259	12.226	13.185

5. Conclusion

A simple NURBS-based isogeometric plate formulation based on the third-order shear deformation theory has been developed for static, bucking, and free vibration analysis of the laminated composite plates. The quadratic, cubic, and quartic elements are utilized to compute displacement, stress, frequencies, and the critical buckling load. The results of the present

Table 10. Normalized critical buckling load of cross-ply [0°/90°] and $[0°/90°]_5$ square plate with various mixed boundaries ($E_1/E_2 = 40$; $a/h = 10$)

Number layer	Method	Boundary condition SSSS	SSFF	SSCC	SSSC	SSFC	SSFS
[0°/90°]	Quadratic	11.5360	4.9374	20.7085	16.8729	6.3487	5.4423
	Cubic	11.5315	4.9350	20.5946	16.8151	6.3397	5.4396
	Quartic	11.5312	4.9348	20.5115	16.7732	6.3330	5.4393
	MISQ20 [86]	11.291	4.860	20.082	16.470	6.140	5.342
	MLSDQ [89]	11.301	4.823	19.871	—	—	—
	RKPM [90]	11.582	4.996	20.624	16.872	6.333	5.502
	FSDT [91]	11.353	4.851	20.067	16.437	6.166	5.351
	HSDT [91]	11.562	4.940	21.464	17.133	6.274	5.442
$[0°/90°]_5$	Quadratic	25.2697	12.0472	35.2311	32.8949	14.3733	12.4783
	Cubic	25.2649	12.0442	35.2151	32.8837	14.3385	12.4751
	Quartic	25.2653	12.0441	35.2091	32.8799	14.3167	12.4748
	MISQ20 [86]	25.525	12.131	35.105	32.870	14.352	12.541
	MLSDQ [89]	25.338	12.030	34.604	—	—	—
	RKPM [90]	25.703	12.224	35.162	32.950	14.495	12.658
	FSDT [91]	25.450	12.092	34.837	32.614	14.358	12.524
	HSDT [91]	25.423	12.077	35.376	32.885	14.351	12.506

Table 11. Biaxial critical buckling load of simply supported cross-ply [0°/90°/0°] square plate with various modulus ratios

Method	E_1/E_2 10	20	30	40
Quadratic	4.9777	7.5446	8.9429	10.1096
Cubic	4.9766	7.5429	8.9383	10.1046
Quartic	4.9765	7.5429	8.9377	10.1040
MISQ20 [86]	4.939	7.488	9.016	10.252
FSDT [92]	4.963	7.588	8.575	10.202
HSDT [85]	4.963	7.516	9.056	10.259

Table 13. A nondimensional frequency parameter $\varpi = (\omega a^2/h)(\rho/E_2)^{1/2}$ of a [0/90/90/0] SSSS laminated plate ($a/b = 1$)

Method	Control point per side	E_1/E_2 10	20	30	40
Quadratic	9	8.3196	9.5816	10.3276	10.8423
	13	8.3152	9.5768	10.3228	10.8374
	17	8.3140	9.5754	10.3213	10.8358
	9	8.3153	9.5766	10.3224	10.8369
Cubic	13	8.3135	9.5747	10.3203	10.8346
	17	8.3131	9.5742	10.3198	10.8340
	9	8.3144	9.5755	10.3211	10.8354
Quartic	13	8.3134	9.5744	10.3200	10.8342
	17	8.3131	9.5741	10.3197	10.8339
RBF [95]		8.2526	9.4974	10.2308	10.7329
Wavelets [96]		8.2794	9.5375	10.2889	10.8117
Global [67]		8.2745	9.5321	10.2814	10.8012
Local [68]		8.3056	9.5804	10.3438	10.8759
Liew [94]		8.2924	9.5613	10.320	10.849
Exact [29, 93]		8.2982	9.5671	10.326	10.854

Table 14. A nondimensional frequency parameter $\varpi = (\omega a^2/h)(\rho/E_2)^{1/2}$ of a [0/90/0] SSSS laminated plate with various ratios a/h

Method	a/h 2	5	10	100
Quadratic	5.4023	10.2879	14.7134	18.8341
Cubic	5.3998	10.2861	14.7114	18.8299
Quartic	5.3995	10.286	14.7113	18.8287
Liew [94]	5.205	10.290	14.767	18.769
Reddy [29]	5.205	10.290	14.767	18.891
Ferreira [98]	5.211	10.307	14.804	18.355
Xiang [99]	5.744	10.475	14.817	18.787

approach are very well compared with those of other existing methods. In particular, the method can predict more accurately than most methods the interlaminar stress of laminated plates even for coarse meshes. One of the advantages of the present method is to increase easily the order of basic functions. By embedding the well-known finite element in to an isogeometric framework, the advantage of exact geometry representation on the first coarsest mesh is inherited. The exact geometry representation is preserved throughout the refinement process without the need for additional communication with the CAD program.

References

[1] N.J.Pagano, Exact solutions for rectangular bidirectional composites and sandwich plates, J. Compos. Mater., vol.4, pp. 20–34, 1970.

[2] S. Srinivas, C.V.Joga, and A.K. Rao, An exact analysis for vibration of simply-supported homogeneous and laminated thick rectangular plates, J. Sound Vib., vol.12, pp. 187–199, 1970.

[3] S. Srinivas and A.K. Rao, Bending, vibration and buckling of simply supported thick orthotropic rectangular plates and laminates, Int. J. Solids Struct., vol. 6, pp. 1463–1481, 1970.

[4] S.S. Vel and R.C. Batra, Analytical solution for rectangular thick laminated plates subjected to arbitrary boundary conditions, AIAA J., vol. 37, pp. 1464–1473, 1999.

[5] A.K. Noor, Free vibration of multilayered composite plates, AIAA J., vol. 11, pp. 1038–1039, 1973.

[6] A.K. Noor, Stability of multilayered composite plates, Fib. Sci. Technol., vol. 8, pp. 81–89, 1975.

[7] E. Reissner and Y. Stavsky, Bending and stretching of certain types of aelotropic elastic plates, J. Appl. Mech., vol. 28, pp. 402–408, 1961.

[8] Y. Stavsky, Bending and stretching of laminated aelotropic plates, J. Eng. Mech. Div., vol. 87, pp. 31–56, 1961.

[9] S.B. Dong, K.S. Pister, and R.L. Taylor, On the theory of laminated anisotrophic plates and shells, J. Aeronaut. Sci., vol. 29, no. 8, pp. 969–975, 1962.

[10] J.M. Whitney, The effect of transverse shear deformation in the bending of laminated plates, J. Compos. Mater., vol. 3, pp. 534–547, 1969.

[11] E. Reissner, A consistent treatment of transverse shear deformations in laminated anisotropic plates, AIAA J., vol. 10, no. 5, pp. 716–718, 1972.

[12] L. Librescu, On the theory of anisotropic elastic shells and plates, Int. J. Solids Struct., vol. 3, no. 1, pp. 53–68, 1967.

[13] M. Levinson, An accurate, simple theory of the statics and dynamics of elastic plates, Mech. Res. Commun., vol. 7, no. 6, pp. 343–350, 1980.

[14] A. Bhimaraddi and L.K. Stevens, A higher order theory for free vibration of orthotropic, homogeneous and laminated rectangular plates, J. Appl. Mech., Trans. ASME, vol. 51, no. 1, pp. 195–198, 1984.

[15] J.N. Reddy, A simple higher-order theory for laminated composite plates, J. Appl. Mech., vol. 51, pp. 745–752, 1984.

[16] J.G. Ren, A new theory of laminated plate, Compos. Sci. Technol., vol. 26, pp. 225–239, 1986.

[17] T. Kant and B.N. Pandya, A simple finite element formulation of a higher-order theory for unsymmetrically laminated composite plates, Compos. Struct., vol. 9, no. 3, pp. 215–264, 1988.

[18] P.R. Mohan, B.P. Naganarayana, and G. Prathap, Consistent and variationally correct finite elements for higher-order laminated plate theory, Compos. Struct., vol. 29, no. 4, pp. 445–456, 1994.

[19] N.J. Pagano and R.S. Soni, Global-local laminate variational model, Int. J. Solids Struct., vol. 19, pp. 207–228, 1983.

[20] W. Zhen and C. Wanji, Free vibration of laminated composite and sandwich plates using global-local higher-order theory, J. Sound Vib., vol. 298, pp. 333–349, 2006.

[21] M. Touratier, An efficient standard plate theory, Int. J. Eng. Sci., vol. 29, no. 8, pp. 901–916, 1991.

[22] M. Karama, K.S. Afaq, and S. Mistou, Mechanical behaviour of laminated composite beam by new multi-layered laminated composite structures model with transverse shear stress continuity, Int. J. Solids Struct., vol. 40, pp. 1525–1546, 2003.

[23] K.P. Soldatos, A transverse shear deformation theory for homogeneous monoclinic plates. Acta Mech., vol. 94, pp. 195–200, 1992.

[24] M. Aydogdu, A new shear deformation theory for laminated composite plates, Compos. Struct., vol. 89, pp. 94–101, 2009.

[25] N.E. Meiche, A. Tounsi, N. Ziane, I. Mechab, and E.A.A. Bedia, A new hyperbolic shear deformation theory for buckling and vibration of functionally graded sandwich plate, Int. J. Mech. Sci., vol. 53, pp. 237–247, 2011.

[26] J.N. Reddy, A refined nonlinear theory of plates with transverse shear deformation, Int. J. Solids Struct., vol. 20, no. 9–10, pp. 881–906, 1984.

[27] R.P. Shimpi, Refined plate theory and its variants, AIAA J., vol. 40, no. 1, pp. 137–146, 2002.
[28] R.P. Shimpi and H.G. Patel, A two variable refined plate theory for orthotropic plate analysis, Int. J. Solids Struct., vol. 43, no. 22, pp. 6783–6799, 2006.
[29] J.N. Reddy, Mechanics of Laminated Composite Plates: Theory and Analysis, CRC Press, Boca Raton, New York, 1997.
[30] J.N. Reddy, Mechanics of laminated composite plates and shells theory and analysis, Second Edition, CRC Press, New York, 2004.
[31] A.D. Reis, E.L. Albuquerque, F.L. Torsani, L.J. Palermo, and P. Sollero, Computation of moments and stresses in laminated composite plates by the boundary element method, Eng. Anal. Bound. Elem., vol. 35, pp. 105–113, 2011.
[32] W.P. Paiva, P. Sollero, and E.L. Albuquerque, Modal analysis of anisotropic plates using the boundary element method, Eng. Anal. Bound. Elem., vol. 35, pp. 1248–1255, 2011.
[33] H. Nguyen-Xuan, T. Rabczuk, Stephane Bordas, and J.F. Debongnie, A smoothed finite element method for plate analysis, Comput. Methods Appl. Mech. Eng., vol. 197, pp. 1184–1203, 2008.
[34] H. Nguyen-Xuan, T. Rabczuk, N. Nguyen-Thanh, T. Nguyen-Thoi, and S.P.A. Bordas, A node-based smoothed finite element method (NS-FEM) for analysis of Reissner-Mindlin plates, Comput. Mech., vol. 46, pp. 679–701, 2010.
[35] H. Nguyen-Xuan, G.R. Liu, C. Thai-Hoang, and T. Nguyen-Thoi, An edge-based smoothed finite element method (ES-FEM) with stabilized discrete shear gap technique for analysis of Reissner-Mindlin plates, Comput. Methods Appl. Mech. Eng., vol. 199, pp. 471–489, 2010.
[36] N. Nguyen-Thanh, T. Rabczuk, H. Nguyen-Xuan, and S. Bordas, A smoothed finite element method for shell analysis, Comput. Methods Appl. Mech. Eng., vol. 198, no. 2, pp. 165–177, 2008.
[37] C. Thai-Hoang, N. Nguyen-Thanh, H. Nguyen-Xuan, T. Rabczuk, and S. Bordas, A smoothed finite element method for free vibration and buckling analysis of shells, KSCE J. Civ. Eng., vol. 15, no. 2, pp. 347–361, 2011.
[38] C. Thai-Hoang, N. Nguyen-Thanh, H. Nguyen-Xuan, and T. Rabczuk, An alternative alpha finite element method with discrete shear gap technique for analysis of laminated composite plates, Appl. Math. Comput., vol. 217, no. 17, pp. 7324–7348, 2011.
[39] T. Rabczuk and T. Belytschko, Cracking particles: A simplified meshfree methods for arbitrary evolving cracks, Int. J. Numer. Methods Eng., vol. 61, pp. 2316–2343, 2004.
[40] T. Rabczuk, S.P. Xiao, and M. Sauer, Coupling of meshfree methods with finite elements: Basic concepts and test results, Comm. Numer. Methods Eng., vol. 22, pp. 1031–1065, 2006.
[41] T. Rabczuk and P.M.A. Areias, A meshfree thin shell for arbitrary evolving cracks based on an external enrichment, Comput. Methods Appl. Mech. Eng., vol. 16, no. 2, pp. 115–130, 2006.
[42] T. Rabczuk and T. Belytschko, A three dimensional large deformation meshfree method for arbitrary evolving cracks, Comput. Methods Appl. Mech. Eng., vol. 196, pp. 2777–2799, 2007.
[43] T. Rabczuk, P.M.A. Areias, and T. Belytschko, A meshfree thin shell method for non-linear dynamic fracture, Int. J. Numer. Methods Eng., vol. 72, pp. 524–548, 2007.
[44] T. Rabczuk and E. Samaniego, Discontinuous modelling of shear bands with adaptive meshfree methods, Comput. Methods Appl. Mech. Eng., vol. 197, pp. 641–658, 2008.
[45] T.J.R. Hughes, J.A. Cottrell, and Y. Bazilevs, Isogeometric analysis: CAD, finite elements, NURBS, exact geometry and mesh refinement, Comput. Methods Appl. Mech. Eng., vol. 194, no. 39–41, pp. 4135–4195, 2005.
[46] S. Lipton, J.A. Evans, Y. Bazilevs, T. Elguedj, and T.J.R. Hughes, Robustness of isogeometric structural discretizations und severe mesh distortion, Comput. Methods Appl. Mech. Eng., vol. 199, no. 5–8, pp. 357–373, 2010.
[47] M. Bischoff and R. Echter, Numerical efficiency, locking and unlocking of NURBS finite elements, Comput. Methods Appl. Mech. Eng., vol. 199, no. 5–8, pp. 374–382, 2010.
[48] H.-J. Kim, Y.-D. Seo, and S.-K. Youn, Isogeometric analysis for trimmed cad surfaces, Comput. Methods Appl. Mech. Eng., vol. 198, no. 37–40, pp. 2982–2995, 2009.
[49] J.A. Cottrell, T.J.R. Hughes, and Y. Bazilevs, Isogeometric Analysis Toward Integration of CAD and FEA, Wiley, Singapore, Singapore, 2009.
[50] I. Akkerman, Y. Bazilevs, V.M. Calo, T.J.R. Hughes, and S. Hulshoff, The role of continuity in residual-based variational multiscale modeling of turbulence, Comput. Mech., vol. 41, pp. 371–378, 2008.
[51] Y. Bazilevs, V.M. Calo, T.J.R. Hughes, and Y. Zhang, Isogeometric fluid-structure interaction: Theory, algorithms, and computations, Comput. Mech., vol. 43, pp. 3–37, 2008.
[52] T.J.R. Hughes, A. Reali, and G. Sangalli, Duality and unified analysis of discrete approximations in structural dynamics and wave propagation: Comparison of *p*-method finite elements with *k*-method NURBS, Comput. Methods Appl. Mech. Eng., vol. 197, pp. 4104–4124, 2008.
[53] J.A. Cottrell, A. Reali, Y. Bazilevs, and T.J.R. Hughes, Isogeometric analysis of structural vibrations, Comput. Methods Appl. Mech. Eng., vol. 195, pp. 5257–5297, 2006.
[54] W.A. Wall, M.A. Frenzel, and C. Cyron, Isogeometric structural shape optimization, Comput. Methods Appl. Mech. Eng., vol. 197, pp. 1976–1988, 2008.
[55] D.J. Benson, Y. Bazilevs, M.C. Hsu, and T.J.R. Hughes, Isogeometric shell analysis: The Reissner-Mindlin shell, Comput. Methods Appl. Mech. Eng., vol. 199, pp. 276–289, 2010.
[56] J. Kiendl, K.-U. Bletzinger, J. Linhard, and R. Wüchner, Isogeometric shell analysis with Kirchhoff-Love elements, Comput. Methods Appl. Mech. Eng., vol. 198, pp. 3902–3914, 2009.
[57] J. Kiendl, Y. Bazilevs, M.-C. Hsu, R. Wüchner, and K.-U. Bletzinger, The bending strip method for isogeometric analysis of Kirchhoff-Love shell structures comprised of multiple patches, Comput. Methods Appl. Mech. Eng., vol. 199, pp. 2403–2416, 2010.
[58] P. Fischer, M. Klassen, J. Mergheim, P. Steinmann, and R. Müller, Isogeometric analysis of 2D gradient elasticity, Comput. Mech., vol. 47, pp. 325–334, 2011.
[59] Y. Bazilevs, V.M. Calo, J.A. Cottrell, J.A. Evans, T.J.R. Hughes, S. Lipton, M.A. Scott, and T.W. Sederberg, Isogeometric analysis using T-splines, Comput. Methods Appl. Mech. Eng., vol. 199, no. 5–8, pp. 229–263, 2010.
[60] A. Buffa, D. Cho, and G. Sangalli, Linear independence of the T-spline blending functions associated with some particular T-meshes, Comput. Methods Appl. Mech. Eng., vol. 199, pp. 1437–1445, 2010.
[61] M. Dörfel, B. Juttler, and B. Simeon, Adaptive isogeometric analysis by local h-refinement with T-splines, Comput. Methods Appl. Mech. Eng., vol. 199, pp. 264–275, 2010.
[62] N. Nguyen-Thanh, H. Nguyen-Xuan, S. Bordas, and T. Rabczuk, Isogeometric analysis using polynomial splines over hierarchical T-meshes for two-dimensional elastic solids, Comput. Methods Appl. Mech. Eng., vol. 200, no. 21–22, pp. 1892–1908, 2011.
[63] N. Nguyen-Thanh, J. Kiendl, H. Nguyen-Xuan, R. Wüchner, K.U. Bletzinger, Y. Bazilevs, and T. Rabczuk, Rotation free isogeometric thin shell analysis using PHT-splines, Comput. Methods Appl. Mech. Eng., vol. 200, nos. 47–48, pp. 3410–3424, 2011.
[64] R.N. Simpson, S.P.A. Bordas, J. Trevelyan, and T. Rabczuk, A two-dimensional isogeometric boundary element method for elastostatic analysis, Comput. Methods Appl. Mech. Eng., vol. 209–212, pp. 87–100, 2012.
[65] S.S. Ghorashi, N. Valizadeh, and S. Mohammadi, Extended isogeometric analysis for simulation of stationary and propagating cracks, Int. J. Numer. Methods Eng., vol. 89, no. 9, pp. 1069–1101, 2012.

[66] A.J.M. Ferreira and G.E. Fasshauer, Natural frequencies of shear deformable beams and plates by a RBF-pseudospectral method, Comput. Methods Appl. Mech. Eng., vol. 196, pp. 134–146, 2006.

[67] A.J.M. Ferreira, R.C. Batra, C.M.C. Roque, L.F. Qian, and R.M.N. Jorge, Natural frequencies of functionally graded plates by a meshless method, Compos. Struct., vol. 75, no. 1–4, pp. 593–600, 2006.

[68] C.M.C. Roque, D. Cunha, and A.J.M. Ferreira, A local radial basis functions—Finite differences technique for the analysis of composite plates, Eng. Anal. Bound. Elem., vol. 35, pp. 363–374, 2011.

[69] J.N. Reddy, Introduction to the Finite Element Method, McGraw-Hill, New York, 1993.

[70] G. Akhras, M.S. Cheung, and W. Li, Finite strip analysis for anisotropic laminated composite plates using higher-order deformation theory, Comput. Struct., vol. 52, no. 3, pp. 471–477, 1994.

[71] A.J.M. Ferreira, MATLAB codes for finite element analysis: Solids and structures, Springer, London, 2008.

[72] K.M. Liew, J. Wang, T.Y. Ng, and M.J. Tan, Free vibration and buckling analyses of shear deformable plates based on FSDT meshfree method, J. Sound Vib., vol. 276, pp. 997–1017, 2004.

[73] A.J.M. Ferreira, C.M.C. Roque, A.M.A. Neves, R.M.N. Jorge, C.M.M. Soares, and K.M. Liew, Buckling and vibration analysis of isotropic and laminated plates by radial basis functions, J. Sound Vib., vol. 42, no. 3, pp. 592–606, 2011.

[74] E. Hinton, Numerical Methods and Software for Dynamic Analysis of Plates and Shells, Pineridge Press, Swansea, UK, 1987.

[75] K.M. Liew, C.M. Wang, Y. Xiang, and S. Kitipornchai, Vibration of Mindlin Plates, Elsevier, Amsterdam, Netherlands, 1998.

[76] M. Azhari, S. Hoshdar, and M.A. Bradford, On the use of bubble functions in the local buckling analysis of plate structures by the spline finite strip method, Int. J. Numer. Methods Eng., vol. 48, no. 4, pp. 583–593, 2000.

[77] A.J.M. Ferreira, C.M.C. Roque, and P.A.L.S. Martins, Analysis of composite plates using higher-order shear deformation theory and a finite point formulation based on the multiquadric radial basis function method, Compos. Struct., vol. 34, pp. 627–636, 2003.

[78] C.H. Thai, L.V. Tran, D.T. Tran, T. Nguyen-Thoi, and H. Nguyen-Xuan, Analysis of laminated composite plates using higher-order shear deformation plate theory and node-based smoothed discrete shear gap method, Appl. Math. Model., vol. 36, pp. 5657–5677, 2012.

[79] A.J.M. Ferreira, Analysis of composite plates using a layerwise deformation theory and multiquadrics discretization, Mech. Adv. Mater. Struct., vol. 12, no. 2, pp. 99–112, 2005.

[80] J. Belinha and L.M.J.S.Dinis, Analysis of plates and laminates using the element-free galerkin method, Comput. Struct., vol. 84, pp. 1547–1559, 2006.

[81] J.R. Xiao, D.F. Gilhooley, R.C. Batra, J.W. Gillespie, Jr., and M.A. McCarthy, Analysis of thick composite laminates using a higher-order shear and normal deformable plate theory (HOSNDPT) and a meshless method, Composites Part B, vol. 39, pp. 414–427, 2008.

[82] A.K. Noor and M.D. Mathers, Shear-flexible finite element method of laminated composite plate, Technical report, NASA, 1975.

[83] L. Liu, L.P. Chua, and D.N. Ghista, Mesh-free radial basis function method for static, free vibration and buckling analysis of shear deformable composite laminates, Compos. Struct., vol. 78, pp. 58–69, 2007.

[84] N.D. Phan and J.N. Reddy, Analysis of laminated composite plates using a higher-order shear deformation theory, Int. J. Numer. Methods Eng., vol. 21, pp. 2201–2219, 1985.

[85] A.A. Khdeir and L. Librescu, Analysis of symmetric cross-ply elastic plates using a higher-order theory: Part II: Buckling and free vibration, Compos. Struct., vol. 9, pp. 259–277, 1988.

[86] H. Nguyen-Van, N. Mai-Duy, W. Karunasena, and T. Tran-Cong, Buckling and vibration analysis of laminated composite plate/shell structures via a smoothed quadrilateral flat shell element with in-plane rotations, Comput. Struct., vol. 89, pp. 612–625, 2011.

[87] A. Chakrabarti and A.H. Sheikh, Buckling of laminated composite plates by a new element based on higher order shear deformation theory, Mech. Compos. Mater. Struct., vol. 10, no. 4, pp. 303–317, 2003.

[88] J.N. Reddy and N.D. Phan, Stability and vibration of isotropic, orthotropic and laminated plates according to a higher order shear deformation theory, J. Sound Vib., vol. 89, pp. 157–170, 1985.

[89] Y.Q. Huang and Q.S. Li, Bending and buckling analysis of antisymmetric laminates using the moving least square differential quadrature method, Comput. Methods Appl. Mech. Eng., vol. 193, no. 33–35, pp. 3471–3492, 2004.

[90] J. Wang, K.M. Liew, M.J. Tan, and S. Rajendran, Analysis of rectangular laminated composite plates via FSDT meshless method, Int. J. Mech. Sci., vol. 44, no. 7, pp. 1275–1293, 2002.

[91] J.N. Reddy and A.A. Khdeir, Buckling and vibration of laminated composite plates using various plate theories, AIAA J., vol. 27, no. 12, pp. 1808–1817, 1989.

[92] M.E. Fares and A.M. Zenkour, Buckling and free vibration of non-homogeneous composite cross-ply laminated plates with various plate theories, Compos. Struct., vol. 44, pp. 279–287, 1999.

[93] A. Kdheir, Analysis of symmetric cross-ply elastic plates using a higher-order theory, Part II: Buckling and free vibration, Compos. Struct., vol. 9, pp. 259–277, 1988.

[94] K.M. Liew, Y.Q. Huang, and J.N. Reddy, Vibration analysis of symmetrically laminated plates based on FSDT using the moving least squares differential quadrature method, Comput. Methods Appl. Mech. Eng., vol. 192, no. 19, pp. 2203–2222, 2003.

[95] A.J.M. Ferreira, A formulation of the multiquadric radial basis function method for the analysis of laminated composite plates, Compos. Struct., vol. 59, no. 3, pp. 385–392, 2003.

[96] A.J.M. Ferreira, L.M.S. Castro, and S. Bertoluzza, A high order collocation method for the static and vibration analysis of composite plates using a first-order theory, Compos. Struct., vol. 89, no. 3, pp. 424–432, 2009.

[97] K.M. Liew, Solving the vibration of thick symmetric laminates by Reissner/Mindlin plate theory and the P-Ritz method, J. Sound Vib., vol. 198, pp. 343–360, 1996.

[98] A.J.M. Ferreira, R.M.N. Jorge, and C.M.C. Roque, Free vibration analysis of symmetric laminated composite plates by FSDT and radial basis functions, Comput. Methods Appl. Mech. Eng., vol. 194, pp. 4265–4278, 2005.

[99] S. Xiang and K.M. Wang, Free vibration analysis of symmetric laminated composite plates by trigonometric shear deformation theory and inverse multiquadric RBF, Thin Walled Struct., vol. 47, pp. 304–310, 2009.